

**THEORETICAL AND EXPERIMENTAL STUDIES
OF AIR ENTRAINMENT IN WOUND ROLLS**

By

MICHAEL WILLIAM HOLMBERG

Bachelor of Science

Oklahoma State University

Stillwater, Oklahoma

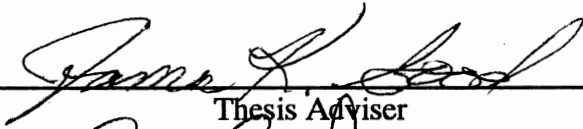
1990

Submitted to the Faculty of the
Graduate School of the
Oklahoma State University
in partial fulfillment of
the requirements for
the Degree of
MASTER OF SCIENCE
May, 1992


Thesis
1992
H747E

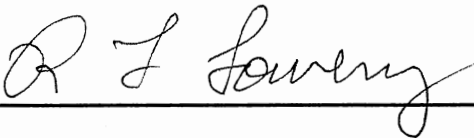
THEORETICAL AND EXPERIMENTAL STUDIES
OF AIR ENTRAINMENT IN WOUND ROLLS

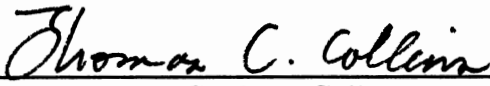
Thesis Approved:



Thesis Adviser







Dean of the Graduate College

ACKNOWLEDGMENTS

I wish to express my thanks and appreciation to my advisor, Dr. James K. Good. His guidance and participation throughout this project have been a tremendous asset. Thanks are also due to my fellow students involved in the Web Handling Research Center; their camaraderie and assistance provide an enjoyable working atmosphere.

I wish to express my appreciation to my parents, Harold and Barbara Holmberg. Their moral and financial support throughout my college career have provided a tremendous amount of help. They have become my greatest role models and it is my hope to eventually attain the success they both have in their personal and business lives.

Most importantly, I would like to thank my loving wife, Allison, for always being understanding and providing the little nudges to keep me going. She has provided the financial means for my graduate program, this enabled a full time commitment to my research. Without her understanding and loving support, I could never have completed or even attempted this endeavor.

TABLE OF CONTENTS

Chapter	Page
I. INTRODUCTION	1
II. LITERATURE SURVEY	3
III. WINDING MODEL SELECTION	6
Altmann Model	8
Pfeiffer Model	11
Hakiel Model	12
IV. EMPIRICAL ANALYSIS OF INNER-LAYER PRESSURE	16
Radial Modulus Stack Tests	16
Experimental Procedures for Empirical Analogies	22
Comparison of Theory and Experiment	23
Describing Deviations Between Theory and Experiment	26
V. MEASUREMENTS OF ENTRAINED AIR	30
Experimental Procedures and Material Selection	30
Comparison of Laser Data and Foil Bearing Theory	38
VI. EXPERIMENTAL DETECTION OF ROLL BODY SLIPPAGE	41
Implementation of Continuous J-Line Printer	42
Experimental Outcomes	43
VII. DETERMINING AIR INDUCED RADIAL MODULUS	45
Modified Stack Test	45
Applying Boyle's Law to the Wound Roll	46
Comparisons of Theory and Experiment	53
VIII. RESULTS AND CONCLUSIONS	58
Future Research	59
REFERENCES	60
APPENDICES	61

Chapter	Page
APPENDIX A - WINDING EXPERIMENTATION.	62
Static Radial Modulus Data	63
Experimental Data for Interlayer Pressures	65
Boundary Condition Results	67
APPENDIX B - LASER EXPERIMENTATION	70

LIST OF TABLES

Table	Page
1. Radial Modulus Polynomial Coefficients Including Air Entrainment	52

LIST OF FIGURES

Figure	Page
1. Air Foil Bearing Configuration	3
2. Wound Roll Air Layer	5
3. Roll Structure Equilibrium Equation	7
4. Instron 8500 and Data Acquisition Setup	17
5. Stress Strain Plot for ICI 92 gage Type-S	18
6. Radial Modulus as Function of Pressure (3rd Order Poly, Fit)	19
7. Radial Modulus as Function of Pressure (Linear Regression)	20
8. Stress Strain Curve with Exponential Fit	20
9. Radial Modulus with $C_0=0$	21
10. 3M Winder Splicer Centerwinding Configuration	22
11. Pull Tab	24
12. Pull Tab Calibration Curve for a 6in Tab ..	24
13. Force Sensitive Resistor (FSR)	25
14. FSR Calibration Curve	25
15. Experimental and Theoretical Radial Pressure Comparison	26
16. Static Measurement Deviations	27
17. Boundary Condition Test Setup	27
18. Boundary Condition Test Results	28
19. Laser Winding Configuration	31
20. Laser Displacement Experimental Setup	32
21. Pile Height Data for 1.18 mil Polypropylene at 50 fpm	33
22. Pile Height Regression for 1.18 mil Polypropylene at 50 fpm	33

Figure	Page
23. Depletion Regressed Data for 1.18 mil Polypropylene at 250 fpm	34
24. Depletion After a Wind at 250 fpm	35
25. Depletion Data for all Velocities	35
26. Depletion Regression After a Wind at 50 fpm	36
27. Depletion Regression After a Wind at 100 fpm	36
28. Depletion Comparison at Center and Edge at 700 fpm	37
29. Air Layer Thickness at 50 fpm	38
30. Air Layer Thickness for Various Velocities	39
31. Comparison of Measured and Theoretical Data at 50 fpm	39
32. Continuous J-Line Printer	41
33. Radial Line Indicating No Roll Body Slippage	42
34. Lines Indicating No Roll Body Slippage	43
35. J-Line Output for 92 gage PET	44
36. J-Line Output for 2.51 mil newsprint	44
37. Radial Modulus Profile via Fluffed Stack Test for ICI 48-S PET.	47
38. Radial Modulus Profile via Fluffed Stack Test for ICI 92-S PET.	47
39. Radial Modulus Profile via Fluffed Stack Test for ICI 200-S PET	48
40. Radial Pressure Profile Comparisons for ICI 48-S PET	48
41. Radial Pressure Profile Comparisons for ICI 92-S PET	49
42. Radial Pressure Profile Comparisons for ICI 200-S PET	49
43. Air Layer Configuration for Boyle's Law	50
44. Radial Pressure Profile Comparisons for ICI 48-S PET	54
45. Radial Pressure Profile Comparisons for ICI 92-S PET	54
46. Radial Pressure Profile Comparisons for ICI 200-S PET	55
47. Air Layer Thickness and Surface Roughness at 50fpm	56

Figure	Page
48. Air Layer Thickness and Surface Roughness at 100fpm	56
49. Air Layer Thickness and Surface Roughness at 250fpm	57
50. Radial Modulus as Function of Pressure for 48 gage	63
51. Radial Modulus as Function of Pressure for 92 gage	64
52. Radial Modulus as Function of Pressure for 200 gage	64
53. Experimental and Theoretical Radial Pressure Comparison 48 gage	65
54. Experimental and Theoretical Radial Pressure Comparison 92 gage	66
55. Experimental and Theoretical Radial Pressure Comparison 200 gage	66
56. Boundary Condition Test Results at 100 fpm	67
57. Boundary Condition Test Results at 160 fpm	68
58. Boundary Condition Test Results at 80 fpm	68
59. Boundary Condition Test Results at 370 fpm	69
60. Pile Height Regression for Wind at 50 fpm	71
61. Pile Height Regression for Wind at 100 fpm	72
62. Pile Height Regression for Wind at 250 fpm	72
63. Pile Height Regression for Wind at 700 fpm	73
64. Depletion Regression for Wind at 50 fpm	73
65. Depletion Regression for Wind at 100 fpm	74
66. Depletion Regression for Wind at 250 fpm	74
67. Depletion Regression for Wind at 700 fpm	75
68. Depletion Regression for Wind at 250 fpm at Edge	75
69. Depletion Regression for Wind at 700 fpm at Edge	76
70. Pile Height Data for Wind at 50 fpm at Center	76
71. Pile Height Data for Wind at 100 fpm at Center	77
72. Pile Height Data for Wind at 250 fpm at Center	77

Figure	Page
73. Pile Height Data for Wind at 700 fpm at Center	78
74. Comparison of Foil Bearing at 50 fpm at Center	78
75. Comparison of Foil Bearing at 100 fpm at Center.....	79
76. Comparison of Foil Bearing at 250 fpm at Center.....	79
77. Comparison of Foil Bearing at 700 fpm at Center.....	80
78. Depletion Data for Various Velocities Measured at Center	80
79. Depletion Data for Various Velocities Measured at Edge	81

NOMENCLATURE

A	Surface Area per Unit Width
C1	Polynomial Coefficient
C2	Polynomial Coefficient
C3	Polynomial Coefficient
CMD	Cross Machine Direction
E	Elastic Modulus (psi)
E_{cm}	Elastic Modulus of the Core Material (psi)
E_r	Modulus in the Radial Direction (psi)
E_t	Modulus in the Tangential Direction (psi)
FSR	Force Sensing Resistor
g^2	E_t / E_r Modulus Ratio
h	Caliper or Grid Spacing (in.)
h_o	Air Layer Thickness (in.)
h_1	Air Layer Thickness (in.)
K_1	Constant in Pfeiffer's Radial Modulus Regression
K_2	Constant in Pfeiffer's Radial Modulus Regression
P	Radial Pressure (Negative Stress in the Radial Direction) (psi)
PH	Pile Height (in)
P_a	Atmospheric Pressure (psi)
P_o	Initial Pressure (psi)
PET	Polyester Film
R_c	Radius of Core (in.)

R	Radius (in.)
r	Radius (in.)
T	Tension (Stress in the Tangential Direction) (psi)
t	Time (seconds)
T, T_w	Winding Tension (Freespan Stress at the Roll Tangent Point) (psi)
u	Radial Displacement (in.)
V	Velocity (in. / second)
ν	Poisson's Ratio
ν_{rt}	Poisson's Ratio in Radial Direction
ν_{tr}	Poisson's Ratio in Tangential Direction
ϵ	Strain (in. / in.)
ϵ_r	Radial Strain (in. / in.)
ϵ_t	Tangential Strain (in. / in.)
θ	Angle in Cylindrical Coordinates (Radians)
σ_r	Stress in the Radial Direction (psi)
σ_t	Stress in the Tangential Direction (psi)

CHAPTER I

INTRODUCTION

The quality of wound rolls depends greatly upon the stresses which are wound into the roll. For instance, the radial stress or pressure within a wound roll must be large enough to sustain the integrity of the wound roll during storage or winding. At another extreme, the winding tension must not be so large that defects such as core collapse or roll buckling (ie. starring) occurs. To date, there exists methods of predetermining the stresses that exist in a roll by knowing a combination of the following parameters; core pressure, web tension, roll radius, and web modulus. By knowing these parameters, a close approximation of the radial pressure can be predicted. Thus, by predetermining the in roll stresses, one is able to determine if the wound web material is going to be subjected to damage.

However, the methods used today to determine interlayer pressures do not incorporate the velocity at which the roll was wound. During the formation of a roll, air is trapped between adjacent layers of the web or media. This trapped air is referred to as AIR ENTRAINMENT. It is believed, and has been experimentally proven in this study, that with increased winding speed the amount of entrained air is also increased. If a large enough amount of air is trapped, then there is no interlayer contact of the material. These layers may ride completely upon air at the roll center (CMD) and transverse directional forces can be resisted. Only at the locations such as roll edges, where the air has escaped, is layer to layer contact possible. This leads to a decreased resistance to circumferential and lateral slippage which may result in some type of roll defect. Therefore, providing an avenue for the roll body defects, mentioned earlier, to occur. If air is being trapped

within the wound roll, then existing winding models are no longer valid. At what speeds does entrained air become a factor? Furthermore, if these speeds are encountered then how does one determine the radial modulus of elasticity in the presence of entrained air? These are questions that this work will address in order to produce a wound roll structure model that encompasses air entrainment.

CHAPTER II

LITERATURE SURVEY

An extensive literature search was performed in order to determine if there exists any material on entrained air in winding. Little information was found on air entrapment in wound rolls. Several papers upon the subject of *AIR FOIL BEARING THEORY* were found.

The first publication of air foil bearing theory was perhaps that of Blok and van Rossum in 1953 [4]. This paper was centered around an experiment using cellophane foil, using oil as the lubricant. “These authors developed a theory based on the assumption that the tape remains straight until such time as it becomes a perfect circle separated from the spindle over an angle of wrap by a constant film thickness”[2]. From this

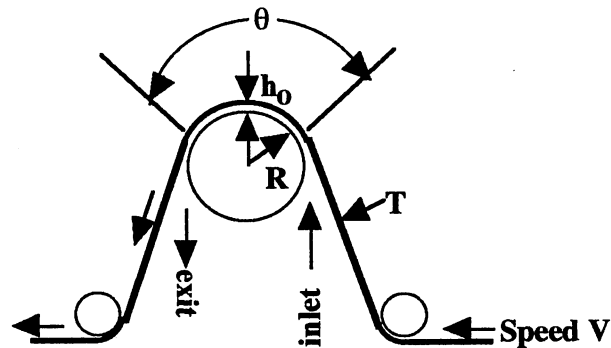


Figure 1. Air Foil Bearing Configuration

assumed film shape, they were able to deduce an expression for the film thickness in the area of uniformity.

In 1965 A. Eshel, presented his paper “The Theory of the Infinitely Wide, Perfectly Flexible, Self-Acting Foil Bearing”. Eshel was interested in using the developments of Blok and Rossum to study the behavior of magnetic media being transported over guiding spindles or recording heads. Figure 1 illustrates the type of problem he analyzed. The media approaches a spindle of radius R at a linear velocity V . As the web passes over the spindle, it entrains an air film and produces a pressure over most of the angle of wrap θ . The problem Eshel wished to analyze was to find the film thickness as a function of web linear velocity, spindle diameter, tension, and any other controlling variables. Below is the analytical equation that Eshel developed for the air film thickness between a moving web and a spindle.

$$h_o = 0.643 R \left(\frac{6\mu V}{T} \right)^{2/3} \quad (1)$$

Where h_o is the air film thickness, R spindle radius, μ dynamic viscosity of air, V web linear velocity, and T web line tension.

The next break through in foil bearing theory was presented by Kenneth L. Knox and Thomas L. Sweeney in 1970 [7]. Knox and Sweeney presented an equation similar to Eshel’s however, Knox and Sweeney’s relationship accounts for a web moving at the same linear velocity as the spindle it travels over. Below is the Knox Sweeney relationship as one can see, the only differences from Eshel’s equation is the constant 6 has been doubled to account for the movement of the spindle and the empirical constant has changed from .643 to .65.

$$h_o = 0.65 R \left(\frac{12\mu V}{T} \right)^{2/3} \quad (2)$$

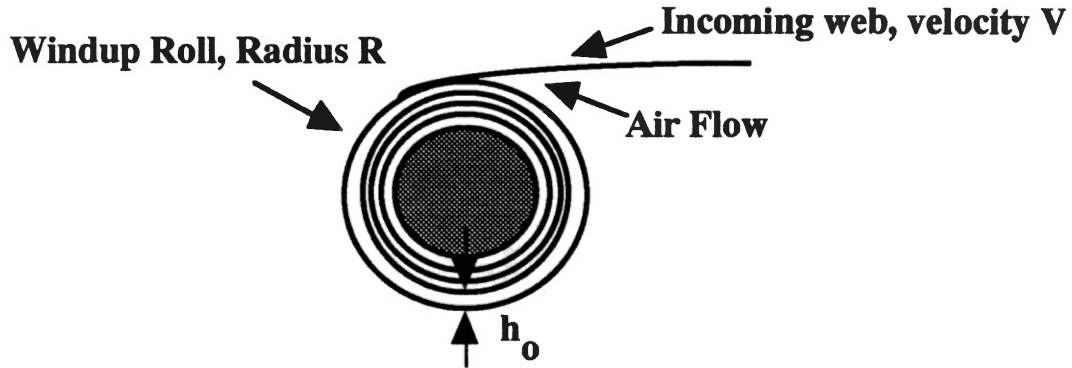


Figure 2. Wound Roll Air Layer

Foil bearing theory has been proven to provide accurate results for a web moving over an idler roll, but can it be utilized for a web entering a wound roll? As a web enters a wound roll, an air layer is formed due to the surface friction of the web material. Then, the air is sandwiched between the outer layer and the previous layer as shown in Figure 2. This configuration has different boundary conditions than what has previously been addressed by air foil bearing theory. Current theories assume the foil bearing is infinitely wide and that side losses are of no consequence. Current theory also requires the inlet and exit pressure to be ambient. These factors question the validity of applying foil bearing theory to the wound roll. However, it may possible to use foil bearing theory as a basis for development of an conservative approximation for entrained air in a wound roll.

CHAPTER III

WINDING MODEL SELECTION

The material properties of the wound roll are nonlinear and exhibit aspects of viscoelasticity. Therefore, to model the interlayer stresses and strains of thousands upon thousands of layers is quite an ordeal. Wound roll models using mechanics formulations were developed over three decades ago [9]. Through time, these models have been developed from the same constitutive relationships into models of today that are representative of true winding. In this chapter, three chronologically ordered models will be introduced; Altmann's model, Pfeiffer's model, and Hakiel's model. It is not the intent of this paper to rederive each of these models but to introduce their importance in history and to present the winding model selected for this project.

A common component found in all winding models is the equilibrium equation. The forces found within a wound roll must balance, therefore the stresses are not independent of each other [10]. The equilibrium equation is derived by summing the contributions of all forces in a radial direction and equating the sum to zero. All shear stresses are assumed to be negligible. The following equation is the equilibrium equation for a cylindrical element in the absence of body forces, as shown in Figure 3.1.

$$r \left(\frac{d\sigma_r}{dr} \right) - \sigma_t + \sigma_r = 0 \quad (3)$$

where:

σ_r = radial stress.

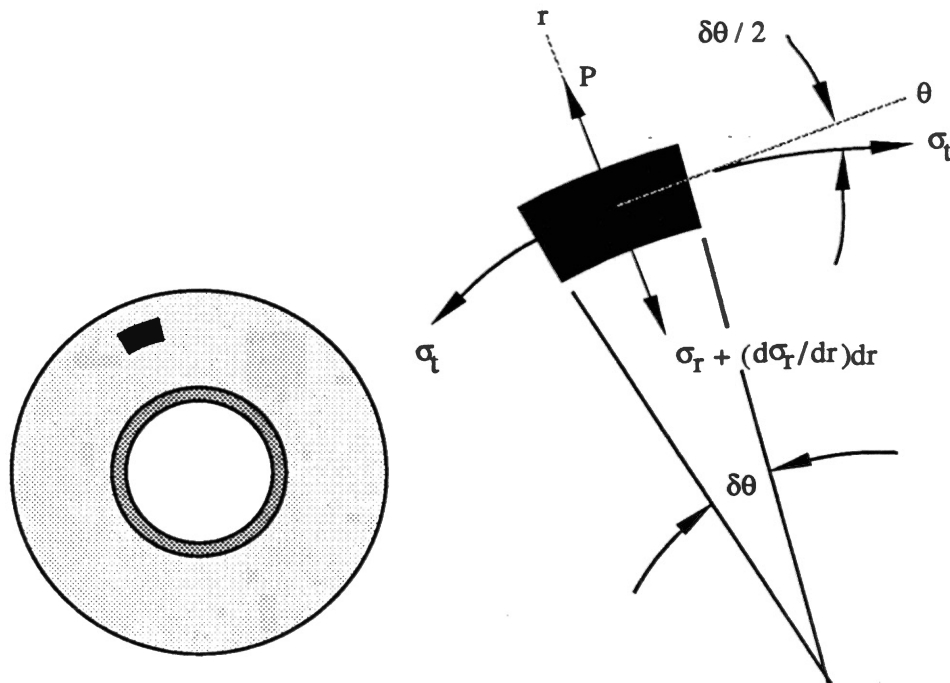


Figure 3. Roll Stress Equilibrium Equation [10]

σ_t = tangential stress.

The equilibrium equation allows the calculation of the circumferential stresses, σ_t , given the radial stress, σ_r , distribution.

Two other components of winding models are the constitutive and compatibility equations. The constitutive equation is developed from Maxwell's relation and Hooke's law. The compatibility equation requires that there are no gaps or voids in the roll and that adjacent laps occupy the same space [10]. By combining the equations of equilibrium, constitutive and compatibility, a second order differential equation describing interlayer stress can be formulated.

In order to solve the second order differential equation, two boundary conditions

are required, one at the core and another at the outer boundary of the roll. The first boundary condition at the core is derived by equating the radial deformation of the first wound on layer and the outside deformation of the core. The second boundary condition is the hoop stress equation and is applied to the outer-most layer. Below are the core and outer boundary conditions respectively:

$$\left. \frac{\partial \delta p}{\partial r} \right|_{r=1} = \left(\frac{E_t}{E_c} - 1 + \nu \right) \delta p \Big|_{r=1} \quad (4)$$

$$P = \frac{T_w h}{r} \quad (5)$$

where,

P = radial pressure.

E_t = tangential modulus of elasticity.

E_c = core stiffness.

r = radius at a point in the roll.

ν = Poisson's ratio of the web.

T_w = winding tension, stress.

h = web caliper.

The next three sections provide a history of winding model development. A good understanding of the development of each of these models is required to enable the evolution of a winding model that incorporates air entrainment.

Altmann Model

In April of 1968, Heinz C. Altmann provided two formulae, the first expresses the

interface pressure and the second provides the in-roll tension stress as a function of the winding tension, the radius ratio to any point of interest in the roll, the outside radius ratio, and the elasticity parameters of web, core, and roll [1]. Altmann used the following assumptions to derive his formulae:

1. The core is cylindrical and remains a cylinder throughout the wind.
2. The thickness of the web is constant and is much smaller than the width of the web, thus provides no resistance to bending.
3. The roll is considered as an homogeneous cylinder throughout the wind, with isotropic properties of radial modulus (E_r), tangential modulus (E_c), radial and tangential components of Poisson's ratio (ν_r, ν_t).
4. Stresses within the roll are a function of radius, not roll angle. This implies that the rate of change of tension is small with respect to web length. This is equivalent to assuming no shear stresses exist.
5. There are no interlayer movements within the roll during the wind. Therefore, there is no roll body slippage allowed in Altmann's model.

With the use of the above assumptions and the following secondary parameters, Altmann developed the first linear anisotropic winding model.

Secondary parameters:

Relative radial compressibility of the roll.

$$\epsilon_r = \frac{E_t}{E_r} \quad (6)$$

Relative radial compressibility of the core.

$$\epsilon_c = \frac{E_t}{E_c} \quad (7)$$

Altmann defined an isotropic component of Poisson's ratio to be:

$$\nu = \frac{1}{2}(\nu_t + \epsilon_r \nu_r) \quad (8)$$

and an anisotropic component of Poisson's ratio to be:

$$\delta = \frac{1}{2}(v_t - \epsilon_r v_r) \quad (9)$$

and,

$$\gamma = \sqrt{\delta^2 + \epsilon_r} \quad (10)$$

$$\alpha = \gamma - \delta \quad (11)$$

$$\beta = \gamma + \delta \quad (12)$$

$$a = \frac{\gamma - v - \epsilon_c}{\gamma + v + \epsilon_c} \quad (13)$$

$$b = 1 - a \quad (14)$$

where,

$\delta, v, \gamma, \alpha, \beta, a$ and b are simplification constants.

With the use of these parameters and governing assumptions, Altmann derived the following anisotropic equations for the wound roll. Equation (15) predicts the interface pressure, P . Equation (16) describes the in-roll tension stress, T , as a function of winding tension, T_w , radius ratio, r , and elastic parameters of the web and core.

$$P = \left(\frac{1 + ar^{2\gamma}}{r^b} \right) \times \int_r^R \left(\frac{s^b}{1 + as^{-2\gamma}} \right) \left(\frac{T_w}{s} \right) ds \quad (15)$$

$$T = T_w - \left(\frac{\alpha - a\beta r^{2\gamma}}{r^b} \right) \times \int_r^R \left(\frac{s^b}{1 + as^{-2\gamma}} \right) \left(\frac{T_w}{s} \right) ds \quad (16)$$

Altmann's relationships revolutionized the analytical approach in analyzing roll body structure. His model is mathematically correct, however, it is limited to the assumption of linearity in the radial-direction modulus of the wound roll. Therefore Altmann's model provided a solid building foundation for the winding models of today.

Pfeiffer Model

In 1966, Pfeiffer introduced the nonlinear compressive behavior of web material in the perpendicular direction to the plane of the web. Pfeiffer approached the wound roll model differently than Altmann. He applied a energy balance technique to help solve the nonlinear compression case [8]. A nonlinear radial modulus is an important concept because it closely models the observed stress-strain behavior in experimental stack tests. In 1968 Pfeiffer presented the following relationship for P_c , core pressure, as a function of K_1 pressure relation multiplier, K_2 basic springiness factor, and ϵ_c compressive strain.

$$P_c = -K_1 + K_1 \exp(K_2 \epsilon_c) \quad (17)$$

Pfeiffer, also describes by a similar analysis, that homogeneous materials, such as plastic or film, may also follow this exponential relationship, stating that at higher pressures the material will begin to behave like a solid [8].

By taking the integral of $P_c d\epsilon_c$, the area under the curve produced by equation (17) can be found as shown below.

$$\xi_c = \int_0^{P_c} -K_1 d\epsilon_c + \int_0^{P_c} K_1 e^{K_2 \epsilon_c} d\epsilon_c = (P_c / K_2) - (K_1 / K_2) \log [(P_c / K_1) + 1] \quad (18)$$

This will define the compressive strain energy of a stack of material compressed from zero to a finite pressure or a finite compressive strain. There is also a steady supply of elastic strain energy coming into the roll. This strain energy is due to the wound-in tension of the roll and is give per cubic volume as:

$$\xi_w = \frac{\sigma^2}{2E_t} \quad (19)$$

By taking into account static equilibrium equation (3) ; Pfeiffer produced a winding stress, σ_e , that has a strain energy equivalent to the local pressure, by multiplying equation (18) by $2E_t$ and taking the square root:

$$\sigma_e = \left(\frac{2E_t P_c}{K_2} - \left(\frac{2E_t K_1}{K_2} \right) \log \left[\left(\frac{P_c}{K_1} \right) + 1 \right] \right)^{\frac{1}{2}} \quad (20)$$

The major importance of this work was incorporating a radial modulus which was a function of pressure, which is realistic for wound rolls.. Pfeiffer's work is an energy balance method, thus it is an approximate method. The stiffness of the core is neglected in this model. His analogies have become a sound basis for comparison through out the ongoing development of theoretical wound roll models.

Hakiel Model

In 1987, Hakiel, developed a nonlinear orthotropic hoop model for the stresses in center wound rolls [4]. Hakiel expanded the works of Altmann and Pfeiffer to produce a theoretical standard from which wound roll stresses in center wound rolls may be analyzed. Furthermore, his model is the basis for comparison in this thesis. Therefore, a

detailed analysis of his model will be given so to understand its assumptions and possible short comings.

Hakiel made the following assumptions in the development of his model:

- 1.) The winding roll is a cylinder made up of a web having uniform width, length, and thickness.
- 2.) The model is composed of winding concentric hoops not spiral formations of the web. During the addition of each hoop the properties of the roll are assumed constant.
- 3.) The roll is assumed to have linear-elastic behavior in the circumferential direction and nonlinear-elastic in the radial direction varying as a function of radial stress as well as being an orthotropic cylinder.
- 4.) The stresses within the roll are not functions of axial or circumferential position, but functions of radial position.
- 5.) Plane stress is assumed and axial components of stress are equal to zero.

Hakiel derives his models by first stating the equilibrium equation for plane stress equation (3), then presenting the linear orthotropic constitutive equations for the radial and tangential directions,

$$\epsilon_r = \left(\frac{1}{E_r}\right)\sigma_r - \left(\frac{\nu_{rt}}{E_t}\right)\sigma_t \quad (21)$$

$$\epsilon_t = \left(\frac{1}{E_t}\right)\sigma_t - \left(\frac{\nu_{tr}}{E_r}\right)\sigma_r \quad (22)$$

Hakiel proceeds by using Maxwell's relation,

$$\frac{\nu_{tr}}{E_r} = \frac{\nu_{rt}}{E_t} \quad (23)$$

to define,

$$v \equiv v_{rt} \quad (24)$$

A Strain compatibility equation is derived from a linear definition of strain in cylindrical coordinates [4] as follows:

radial strain is:
$$\epsilon_r = \frac{\partial u}{\partial r} \quad (25)$$

The circumferential strain is determined by comparing the circumference of one hoop before and after supplying a radial deformation u to the hoop.

$$\epsilon_\theta = \frac{2\pi(u+r) - 2\pi r}{2\pi r} = \frac{u}{r} \quad (26)$$

Where ϵ_θ is the circumferential strain.

$$\frac{\partial \epsilon_\theta}{\partial r} = \frac{\partial}{\partial r} \left(\frac{u}{r} \right) = \frac{\partial u}{r} - \frac{u}{r^2} \quad (27)$$

$$\frac{\partial \epsilon_\theta}{\partial r} = \frac{\epsilon_r}{r} - \frac{\epsilon_\theta}{r} \quad (28)$$

$$r \left(\frac{d\epsilon_r}{dr} \right) + \epsilon_t - \epsilon_r = 0 \quad (29)$$

As described earlier the equations of equilibrium, constitutive, and compatibility may be combine to form the following second order differential equation:

$$r^2 \left(\frac{d^2 \sigma_r}{dr^2} \right) + 3r \left(\frac{d\sigma_r}{dr} \right) - (g^2 - 1) \sigma_r = 0 \quad (30)$$

where,

$$g = \sqrt{\frac{E_t}{E_r}} \quad (31)$$

Hakiel now proceeds to describe an iterative procedure on analyzing the interlayer pressure developed at any radius layer by layer. By letting δP be the interlayer pressure at any radius r evolved by the winding of a single layer of thickness h and tension T_w producing the following form of equation (30):

$$r^2 \left(\frac{d^2 \delta P}{dr^2} \right) + 3r \left(\frac{d \delta P}{dr} \right) - (g^2 - 1) \delta P = 0 \quad (32)$$

Two boundary conditions are need to solve the second order differential equation, one at the core and the other at the outer layer, equations (4) and (5) respectively. Now that a method for computing the stresses in a wound roll as a function of the addition of a single layer has been defined, the total stress distributions within the roll can be determined. By using a finite difference solution of equation (30) a tri-diagonal matrix results which can be solved for stresses within the wound roll.

Hakiel's roll structure was selected as a basis to perform an empirical study of the effects of air entrainment on interlayer pressures in centerwound rolls. Hakiel's model does not include the effects of entrapped air. One may correlate very low winding speed experiments to Hakiel's existing model, at these speeds entrained air is not a factor.

CHAPTER IV

EMPIRICAL ANALYSIS OF INTERLAYER PRESSURE

To empirically study the effects of air entrainment on interlayer pressures in centerwound rolls a web material must be selected. ICI type S, 48, 92, 200 gage polyester were selected for use throughout the experimentation. Polyester is a nonpermeable material and the winding of polyester is influenced by entrained air at lower velocities than permeable materials (i.e. paper). Furthermore, due to the equipment inabilities to wind at speeds greater than 2000 fpm, this study was constrained to nonpermeable materials. This chapter explains the experimental procedures used to analyze interlayer pressures in centerwound rolls. Material properties measurements are discussed first followed by experimental and theoretical comparisons of radial pressures within wound rolls.

Radial Modulus Stack Tests

In order to utilize Hakiel's winding model, various material property data must be collected. The most difficult property to measure is the radial modulus, E_r . For elastic materials E_r is a constant and not a function of stress or strain. However, for web materials E_r is very nonlinear and is a function of many variables (i.e. entrained air, surface roughness of the film, etc.). The Instron 8500 was implemented to evaluate the radial modulus for the three samples of polyester (see Figure 4). Following is a concise outline

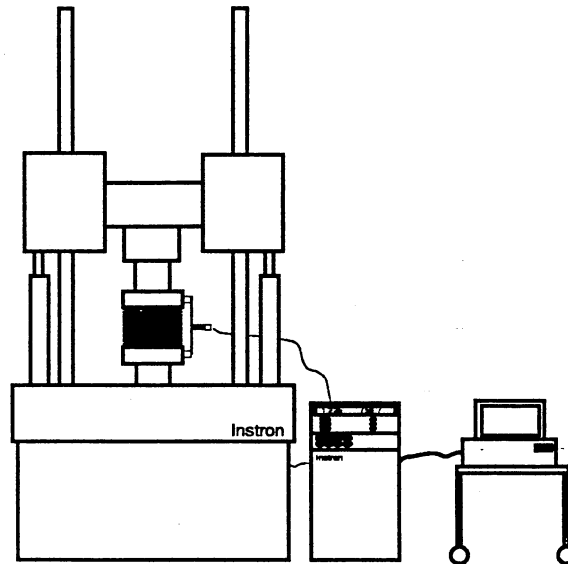


Figure 4. Instron 8500 and Data Acquisition Setup

of the procedures required to measure the radial modulus with the Instron.

- 1.) Material Preparation: Samples of the polyester are cut from stock rolls large enough to over hang the platens on the Instron and produce a pile height of at least one inch.
- 2.) Instron Preparation: First the Instron must be calibrated for load, displacement, and strain control. Next a decision must be made as to whether load or displacement control is to be used. Load control provides data at very even spacing intervals, however it does not provide much information at low pressure regimes [10]. Considering the high interlayer pressures typically found when winding polyester, load control was the chosen testing procedure.
- 3.) Experimentation and Data Acquisition: Computer control of the Instron is provided by a IBM-AT clone with the use of a BASIC program COLLCYCL.BAS. This program allows the user to specify what data is to be collected and at what rate the data will be sampled. Once the program

is started, the Instron can be put under the software's control by depressing the remote button on the Instron. Load, deformation and strain data was collected for ICI type S polyester in three thicknesses (48, 92, and 200 gage). The test load sequence was a triangle shaped load profile beginning at zero and ending at a maximum load of 14,000 pounds.

5.) Two methods of data manipulation were performed to acquire E_r as a function of pressure.

a.) By plotting STRESS versus STRAIN, Figure 5, a 4th order polynomial equation may be fitted to the experimental data, then by taking the derivative of this curve fit equation a 3rd order equation for E_r in terms of radial stress or pressure can be obtained, Figure 6.

b.) A linear regression of several STRESS, STRAIN points can be

$$P = 12.436 - 4.2261e+4 \epsilon + 1.0414e+7 \epsilon^2 - 8.0015e+8 \epsilon^3 + 2.0497e+10 \epsilon^4 \quad R^2 = 0.997$$

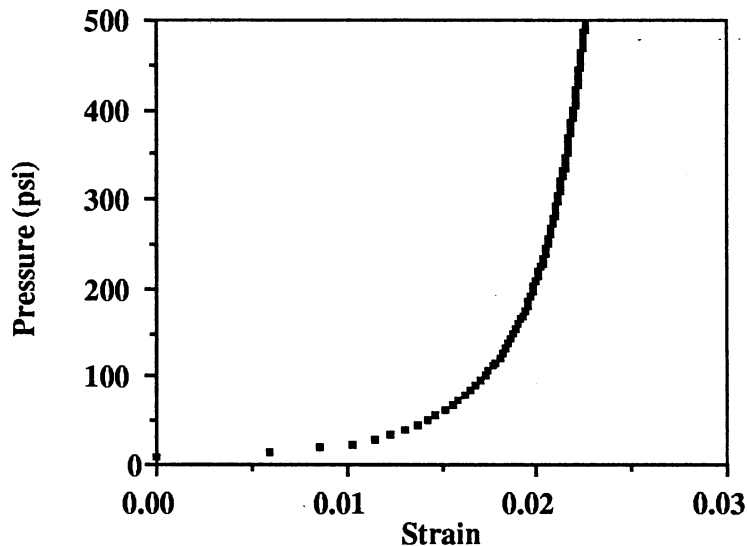


Figure 5. Stress Strain Plot for ICI 92 gage Type-S

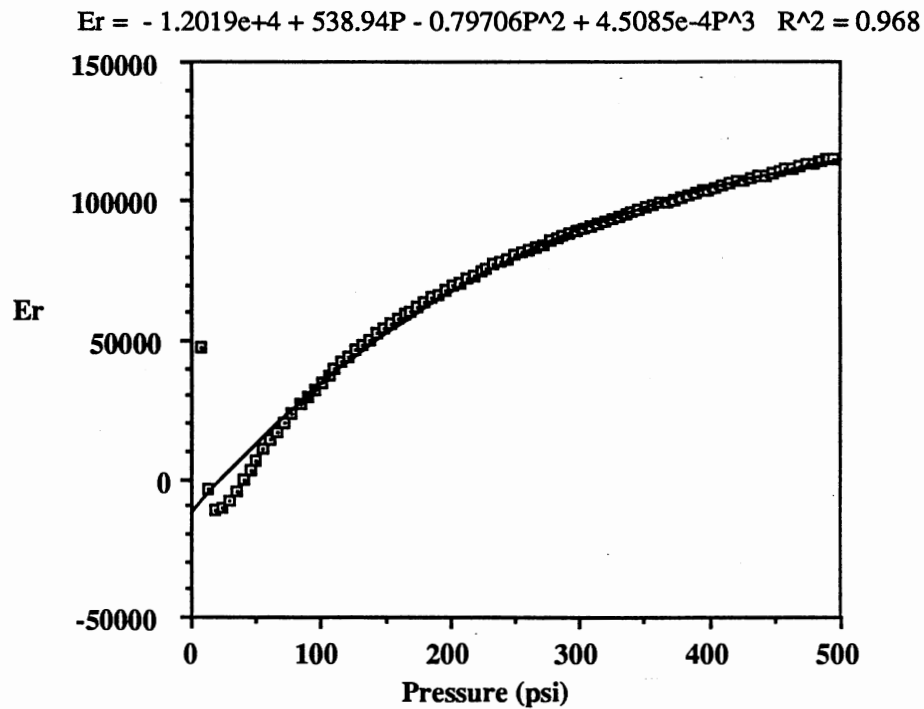


Figure 6. Radial Modulus as Function of Pressure(3rd order Poly. Fit)

evaluated around a specific point this will produce an average value of E_r over a set number of points. Figure 7 shows the result of this method.

In constraining a linear regression of 10 data points an accurate representation at a specific pressure may be made. By applying a polynomial curve fit to all the data as discussed in method (a), one is attempting to minimize error over an entire domain. This will produce less accurate representation at a given pressure. However, an exponential fit produced a lower correlation coefficient, as shown in Figure 8. Appendix A provides the experimental profiles of E_r for all three materials tested.

6.) Since it is impossible to have negative values for radial modulus, the linear regression

$$E_r = -2542.2 + 209.28P + 0.58722P^2 - 5.1623e-4P^3 \quad R^2 = 1.000$$

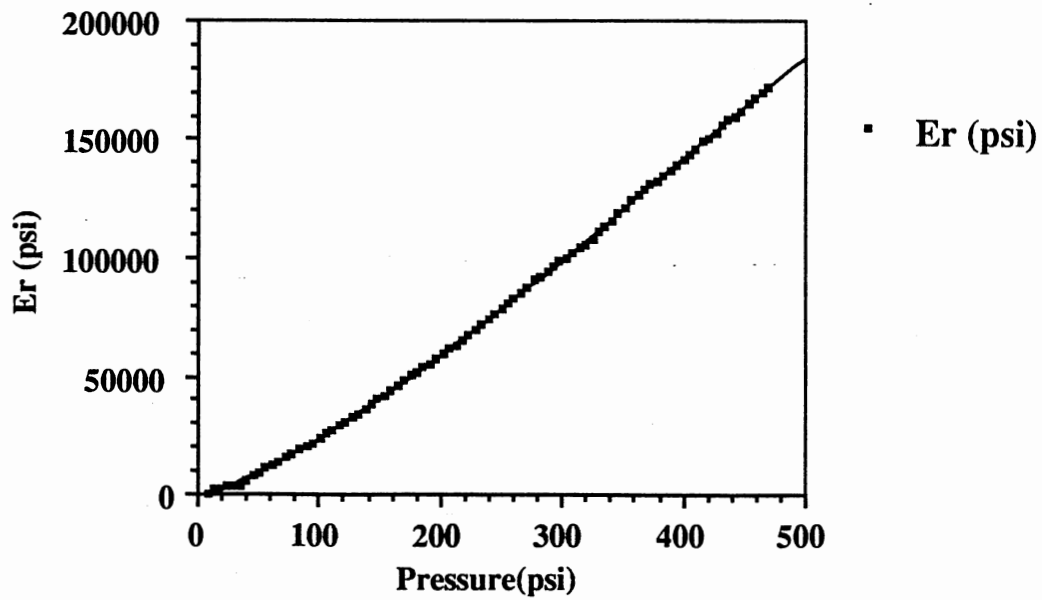


Figure 7. Radial Modulus as Function of Pressure (Linear Regression)

$$y = 2.5302 * 10^{(97.652 \epsilon)} \quad R^2 = 0.956$$

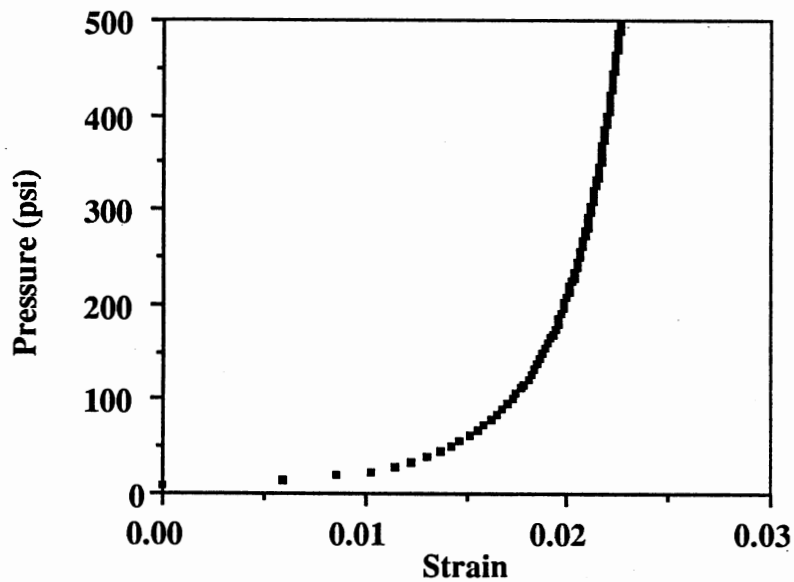


Figure 8. Stress Strain Curve With Exponential Fit

data must curve fit again forcing the intercept term to be zero, Figure 9. This now produces the nonlinear function of E_r required for input in Hakiel's winding model.

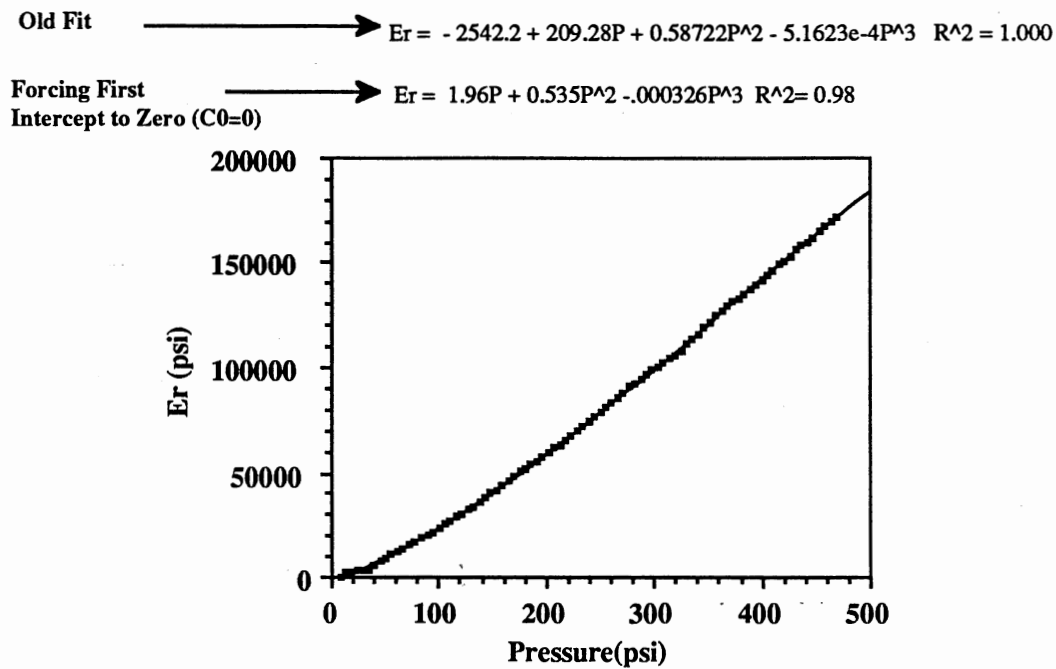


Figure 9. Radial Modulus with $C_0=0$

- 7.) Tangential modulus of elasticity was assumed to be 600,000 psi for this material. This value was arrived at from past measurements of E_t at the Web Handling Research Center [10].

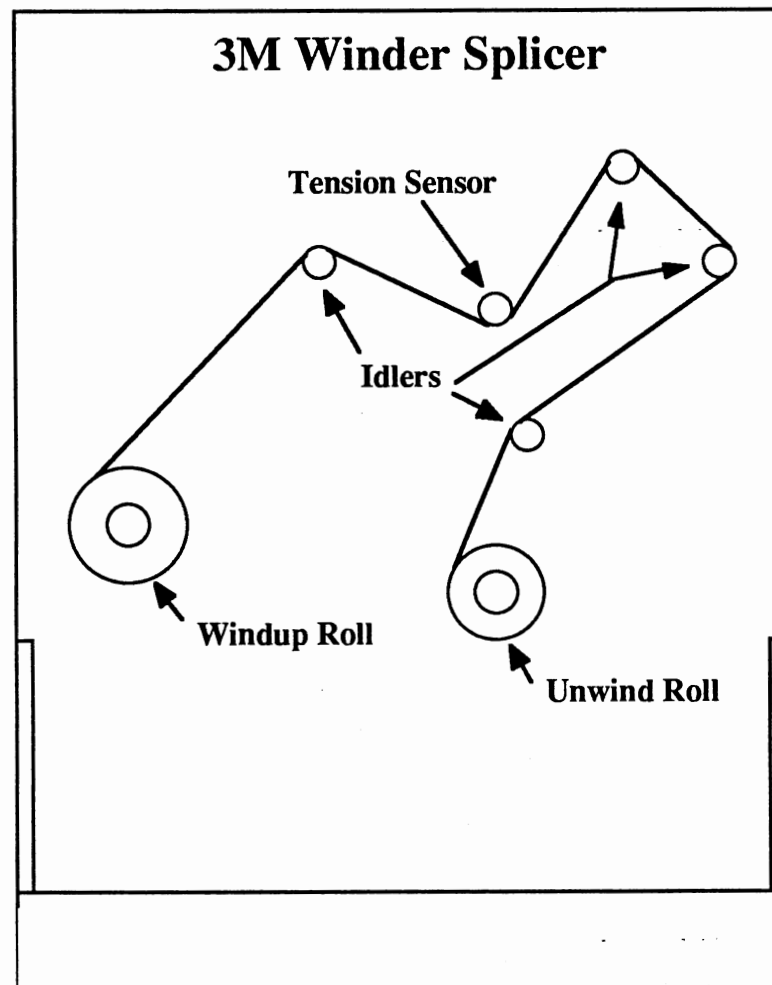


Figure 10. 3M Winder Splicer Centerwinding Configuration

Experimental Procedures for Empirical Analogies

Now that material properties have been defined, experimental winding may be performed to develop a comparison of theory and experiment. Figure 10 shows the winding configuration used for all experiments on the 3M winder. Two methods of acquiring interlayer pressures within a wound roll were used:

- 1.) PULL-TABS (Figure 11): Pull-tabs are a stainless steel feeler gage housed within brass shim stock. By applying a set pressure to the pull-tab, a pull force to cause a slip between the feeler gage and the brass shim can be measured. Thereby, a calibration curve for pressure versus pull force can be generated. Figure 12 shows this calibration for a 6in gage.

and

- 2.) FSR, Force Sensitive Resistor (Figure 13): FSR's are devices that change in resistance due to applied load. As with the pull-tab one could apply a pressure to the surface of the FSR and read a corresponding resistance. Thus a calibration curve on Log-Log axis for pressure versus resistance may be determined as shown in Figure 14.

The devices are inserted into the roll on the fly. As soon as winding is completed pressure profile data is acquired with the use of a digital multimeter and a mechanical force gage. This procedure was applied to numerous experimental winds. Figure 15 provides a typical representation of the experimental results. Appendix A includes all data acquired using the pull-tabs and FSR's.

Comparison of Theory and Experiment

Figure 15 shows a comparison between theory and experiment for 92 gage type Spolyester wound at 50 and 250 fpm. The comparisons of the 48, and 200 gage type S polyester can be found in Appendix A. These figures show two distinct features:

- 1.) As velocity is increased, the radial pressure is decreased.
- 2.) Hakiel's model is over estimating the interlayer pressure within a centerwound roll when significant air has become entrained.

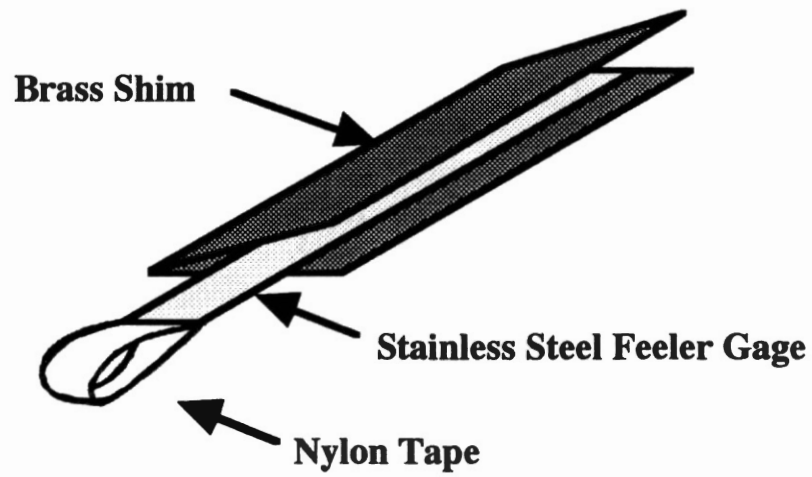


Figure 11. Pull Tab

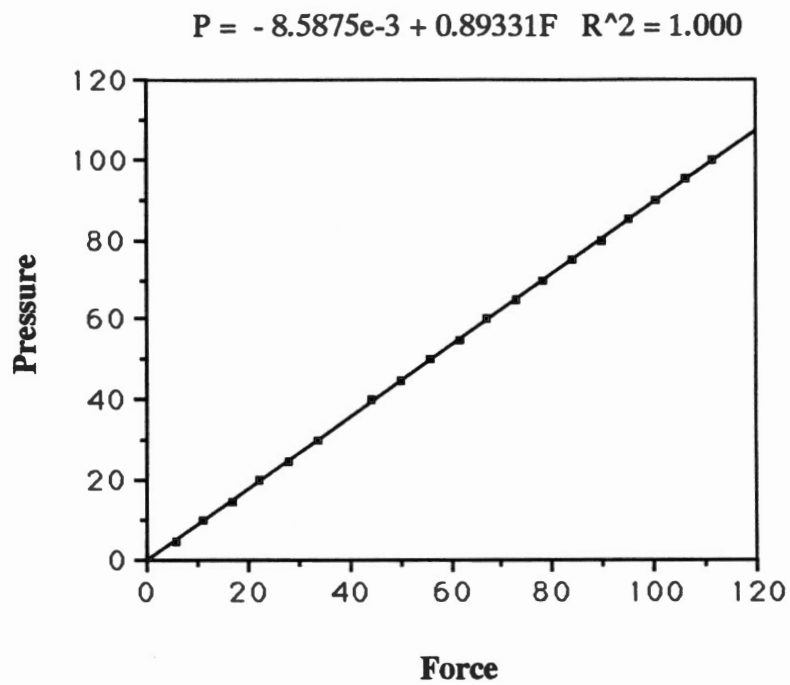


Figure 12. Pull Tab Calibration Curve for a 6in. Tab

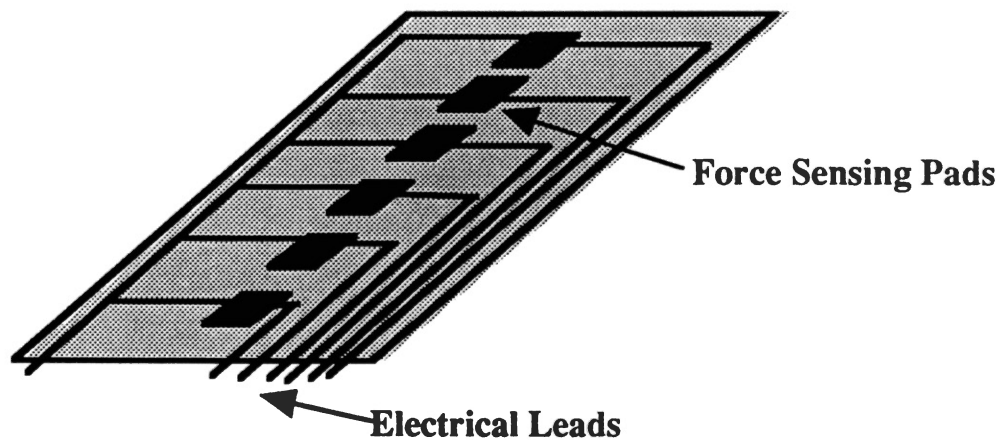


Figure 13. Force Sensitive Resistor (FSR)

$$\text{LOG}(P) = 109.80 - 68.978\text{LOG}(R) + 14.474\text{LOG}(R)^2 - 1.0182\text{LOG}(R)^3 \quad R^2 = 0.950$$

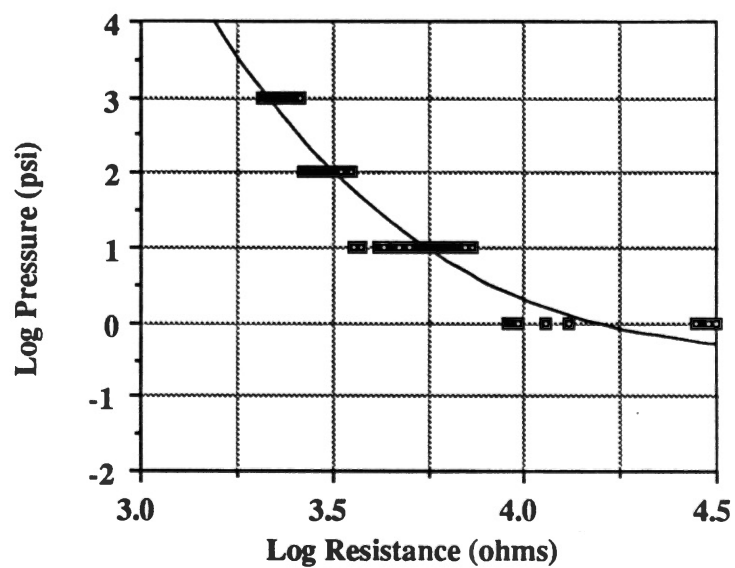


Figure 14. Force Sensitive Resistor (FSR)

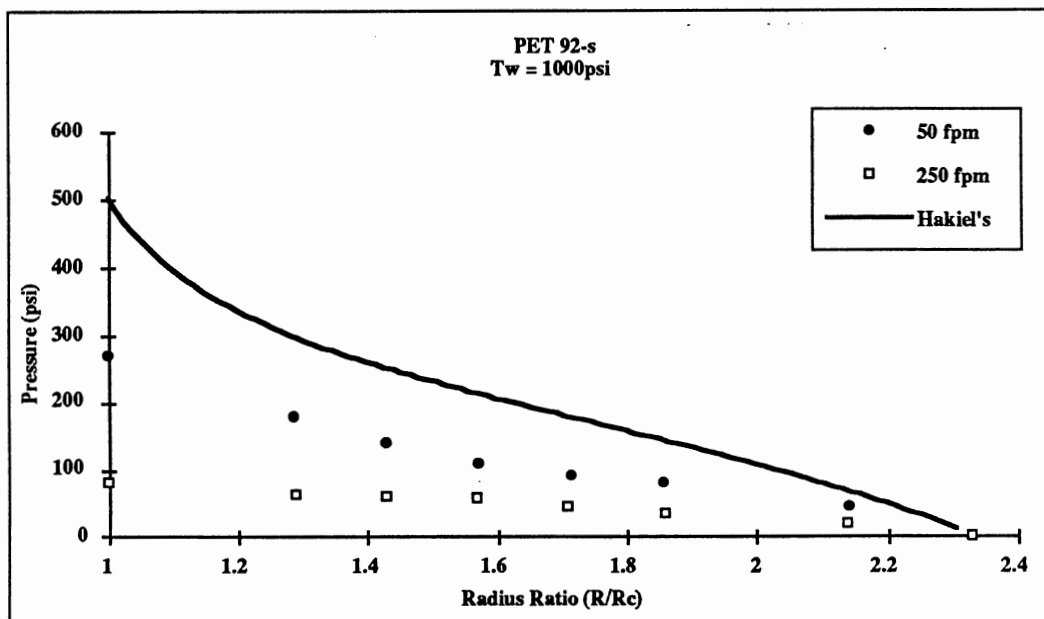


Figure 15. Experimental and Theoretical Radial Pressure Comparison

By assuming that air is entrained and the air layer thickness is a function of velocity, the first observation is easily explained by realizing with more entrained air the roll becomes more spongy thus less supportive of radial loads. Chapter 5 is devoted to proving that air is entrained within the wound roll and that the air layer thickness is a function of velocity.

The second observation can be due to many factors such as incorrect static measurements of E_r and T_w or Hakiel's model is in some way erroneous for variations of speed. The next section is devoted to the understanding of the difference between Hakiel's predicted values and experimental values of radial pressure.

Describing Deviations Between Theory and Experiment

Four potential sources for the difference seen in Figure 15 were identified as

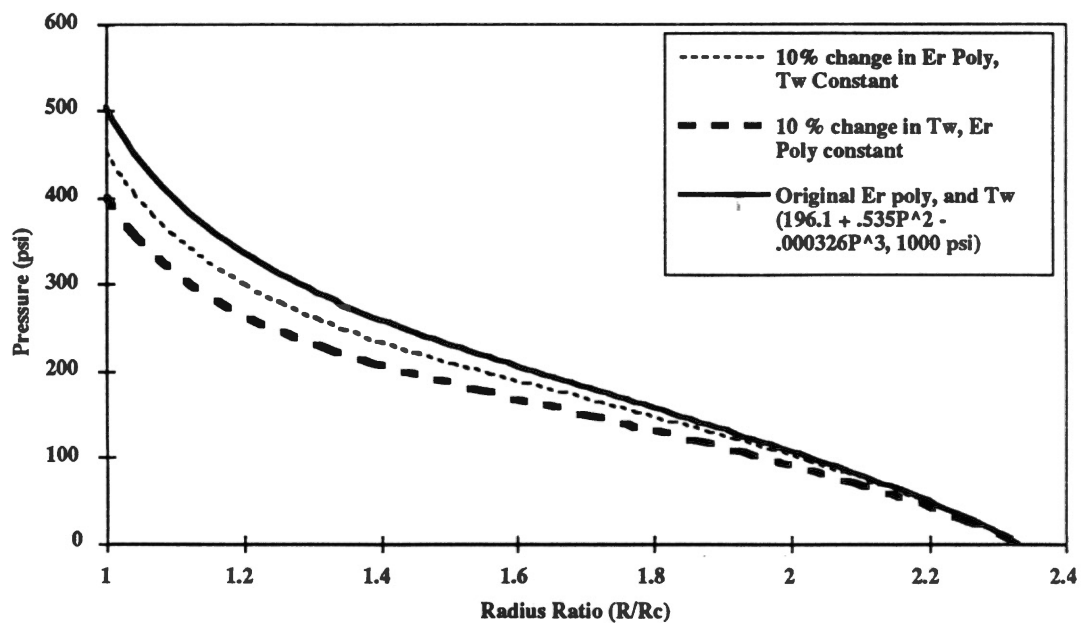


Figure 16. Static Measurement Deviations

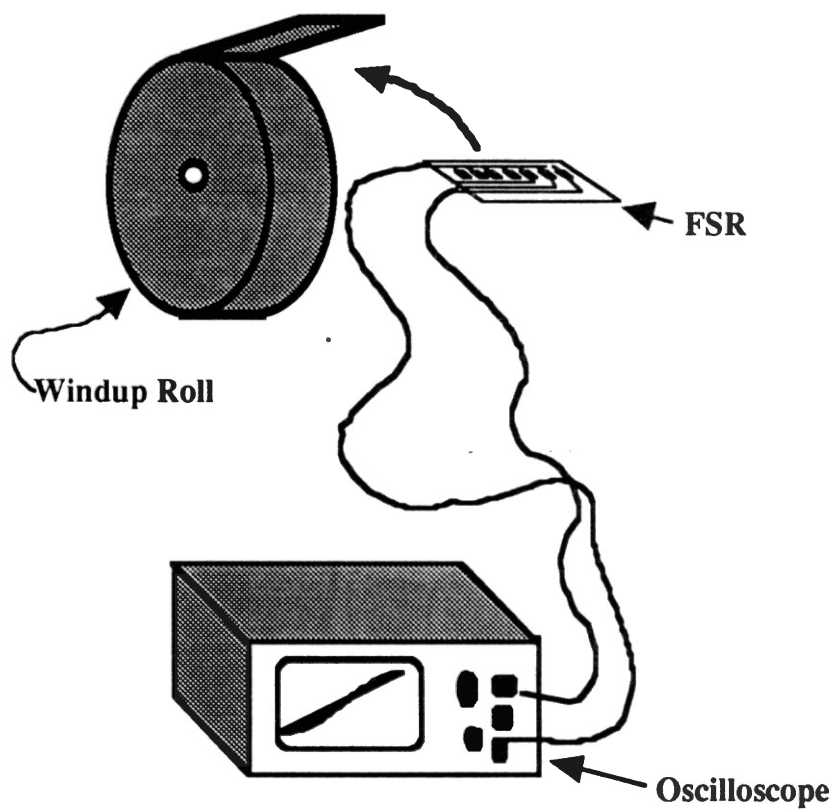


Figure 17. Boundary Condition Test Setup

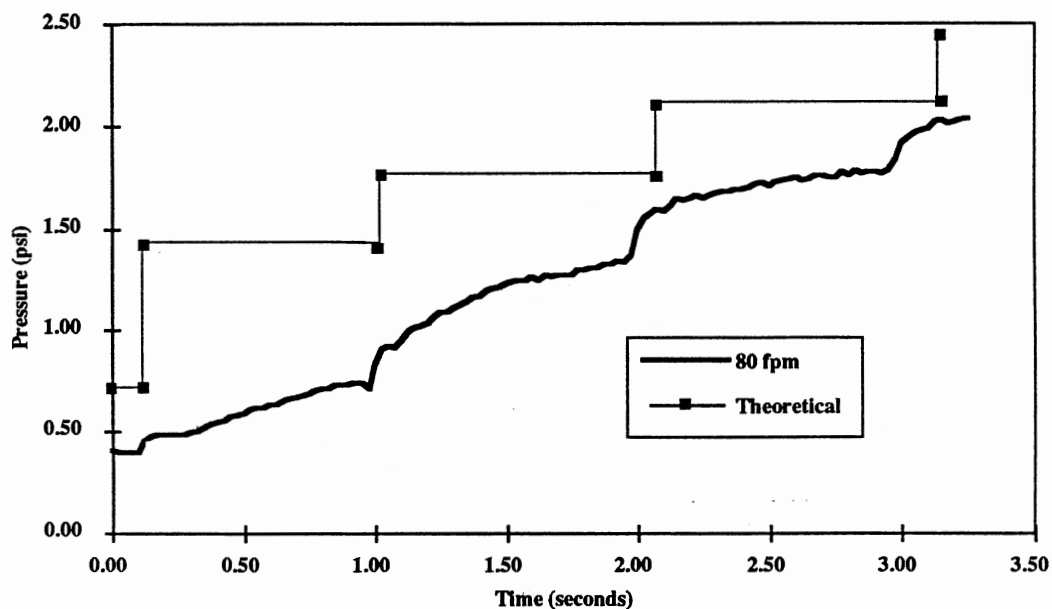


Figure 18. Boundary Condition Test Results

follows: 1.) the measured value of the radial modulus (E_r) was incorrect. 2.) the measured value of the winding tension (T_w) was incorrect, 3.) the outer boundary condition assumed in Hakiel's model is insufficient, and 4.) the measurement of E_r in a static test is insufficient, as will be discussed in chapter 7.

Ranges for potential errors for E_r and T_w were determined ($E_r \pm 10\%$, $T_w \pm 10\%$) and extreme values were used in Hakiel's model. As shown in Figure 16, the resulting pressure profiles could only account for a very small portion of the observed error. Therefore, the boundary condition or incorrect method for obtaining must be the source of the error between Hakiel's result and the experimental data. To analyze the boundary condition, a force sensitive resistor (FSR) was connected to a voltage divider circuit and then attached to an oscilloscope. By winding the FSR into the roll, the pressure of each lap added may be visualized and calculated from the oscilloscope as shown in Figure 17. By using the voltage, FSR resistance, and the duration of the test,

pressure (psi) versus time (seconds) data were derived. Using Hakiel's outer boundary condition (Equation 5), theoretical values of pressure for each lap added may be determined. Figure 18 shows the result of the boundary condition test. This figure clearly shows that Hakiel's outer boundary condition is inadequate when entrained air is present. Applying the same procedure outlined above for various winding speeds, an average 25% loss between the expected and experimental pressures was determined.

This provides proof to the inadequacies found in using the hoop stress relationship as the outer boundary condition when entrained air effects are present. However, if a dynamic E_r value could be determined, then Hakiel's model might correlate better with experimental data. Furthermore, if the air layer thickness for each layer is determined then Hakiel's model may be altered to incorporate effects of entrained air.

CHAPTER V

MEASUREMENTS OF ENTRAINED AIR

Chapter 4 introduced the importance of knowing the amount of air being entrained between the layers of the windup roll at various speeds. This will aid in developing a wound-in-tension correction factor. This data could then be used to estimate a dynamic value of E_T due to entrapped air. This chapter provides the development of measurements of entrained air within centerwound rolls, as well as a comparison to the air foil bearing equation (equation 2).

Experimental Procedures and Material Selection

Laser displacement meters were utilized to measure the change in pile height of a winding roll. If the caliper of the web is assumed constant, one could then back calculate the amount of entrained air layer by layer, or in an entire wound roll. Due to the need to have extremely precise displacement measurements, on the order of $1E-3$ millimeters, the Beloit Two Drum Winder was selected to do all laser experimentation. This winder is equipped with two 2 foot diameter drums that are not out of round more than three thousandths of an inch. This winder was intended to be used as a surface winder, however in this work one of the drums on the winder was utilized as a core for centerwinding configuration (see Figure 19).

The Keyence LC-2100 laser displacement meters were chosen to measure the increasing pile height. These laser sensors are capable of measuring 6 millimeters (mm) of total displacement measurement. These sensors have a resolution of 0.1 micrometers

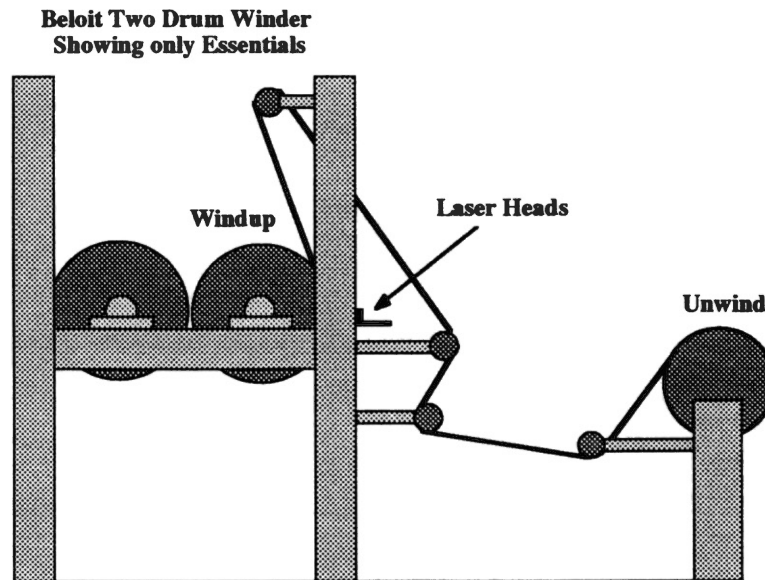


Figure 19. Laser Winding Configuration

and are equipped with digital as well as analog output. Upon initial investigation, on measuring distance from static objects, a reflectivity criteria was developed thereby dictating the material to be used throughout this endeavor. Unfortunately, the clear polyester films used during the experimental winding phase of this work could not be seen by the lasers until a substantial pile height had been accumulated. The laser meters were then measuring to some point beneath the first few layers. Therefore, a white polypropylene provided by Mobil Chemical was utilized as the web material during the laser experimentation. The material was 0.00118 in thick and 11.5 in wide and all testing was done at a constant tension of 1000 psi at various winding speeds. This material provided enough reflectivity for the laser to see a single sheet. This allows accurate measurement of air layer thickness between individual web layers.

A data acquisition package had to be developed to acquire the data from the lasers for analysis. Lab View II, a data acquisition software that allows the user to produce a

virtual instrument for data analysis, was selected as the basis for data acquisition. The laser meters produce 1 volt output for every 1 mm of displacement, thus allowing an electrical analog signal to be read corresponding to distance. By connecting the laser meter to an HP-5413 oscilloscope a displacement profile can be generated for a given

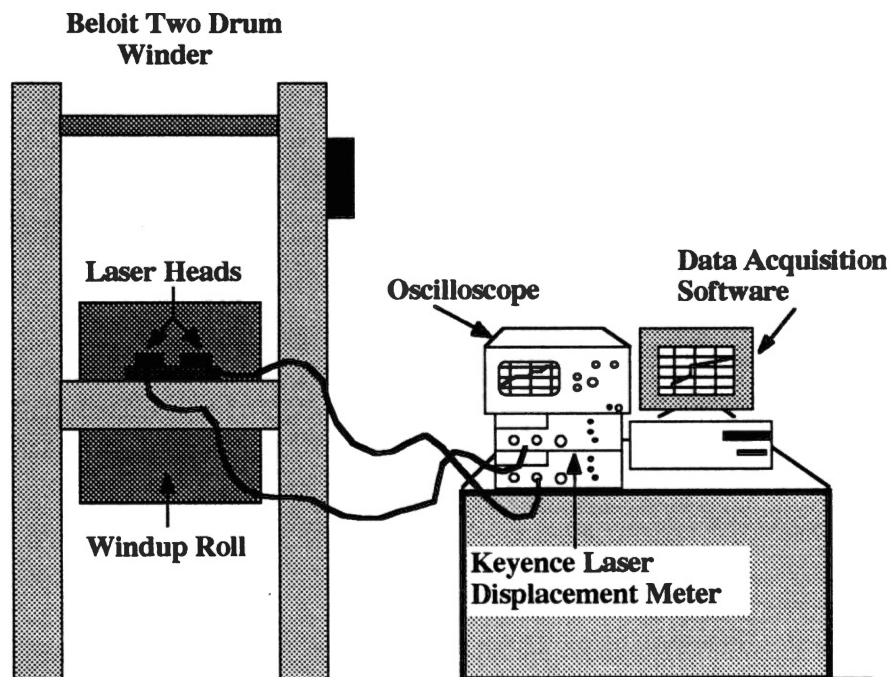


Figure 20. Laser Displacement Experimental Setup

period of time only limited by the constraints of the oscilloscope. With a virtual oscilloscope generated in Lab View II, the displacement profile can be saved for future analysis. Thus, through the use of an HP-5413 oscilloscope and Lab View II, air layer data were obtained. Figure 19 shows the winding configuration for the Beloit Two Drum Winder. Figure 20 shows the experimental setup for this procedure. The setup allows for 50 seconds of pile height data to be measured, as constrained by the oscilloscope, or a

maximum of 6 millimeter of pile height limited by the laser meter. Also, the setup provides the ability to measure the cross machine direction (CMD) air layer profile by simply traversing the laser heads parallel to the wound roll. Figure 21 provides a typical description of the data acquired using the above procedures, where total caliper is the incremental web thickness accumulated after a wind and pile height refers to the mea-

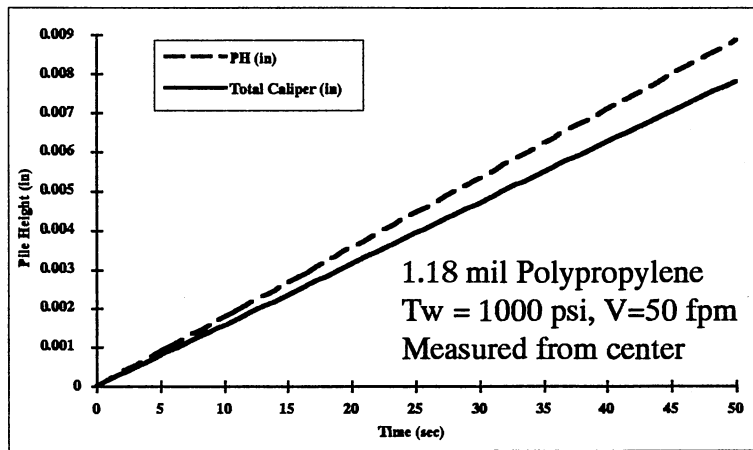


Figure 21. Pile Height Data for 1.18 mil Polypropylene at 50 fpm

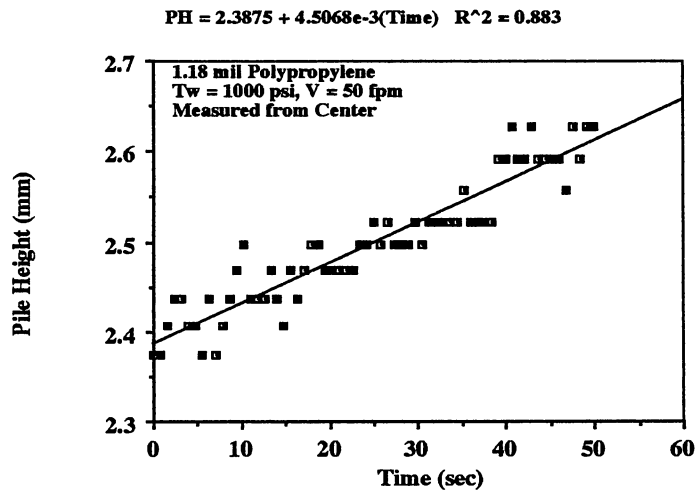


Figure 22. Pile Height Regression for 1.18 mil Polypropylene at 50 fpm

sured web thickness including entrained air. This figure clearly shows that air is being trapped within the roll even at low winding velocities. To develop this figure the experimental data were massaged via a first order linear regression, as shown in Figure 22.

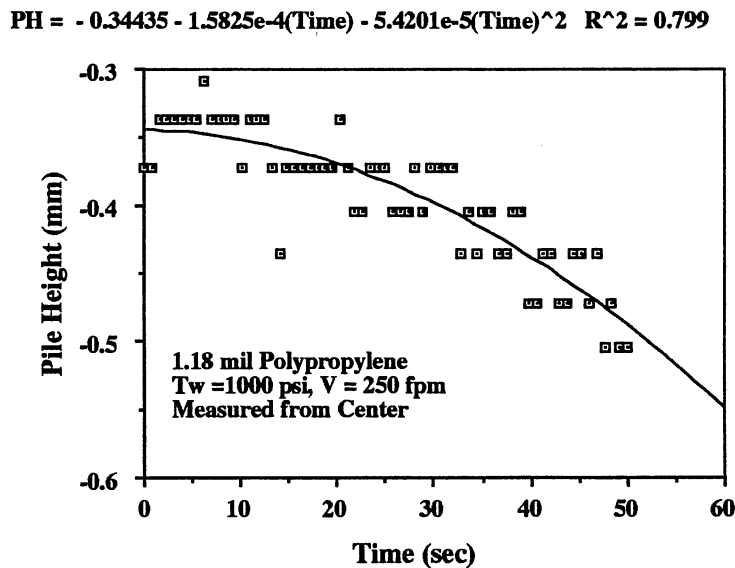


Figure 23. Depletion Regressed Data for 1.18 mil Polypropylene at 250 fpm

Appendix B provides similar results for 100, 250, and 700 fpm experimental winds. To determine if the air remains in the roll over a period of time, or if the air leaks out the sides of the wound roll after winding at various velocities, was accomplished by monitoring the roll with lasers for a sample period. Again, experimental data was regressed, in this case with a second order polynomial. Figure 23 shows the experimental data and the appropriate curve fit for a test after a wind at 250 fpm. This experimentation proves that the air is leaking out of the wound roll over a period of time, thus inducing a relaxation of the wound roll over a period of time. This roll body relaxation may account for the interlayer pressure differences between experiment and theory. Figure 24 represents the

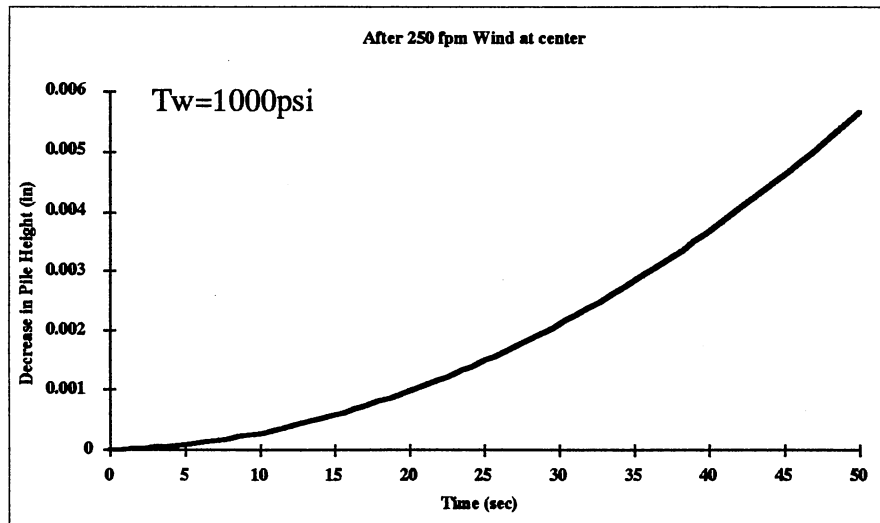


Figure 24. Depletion After a Wind at 250 fpm

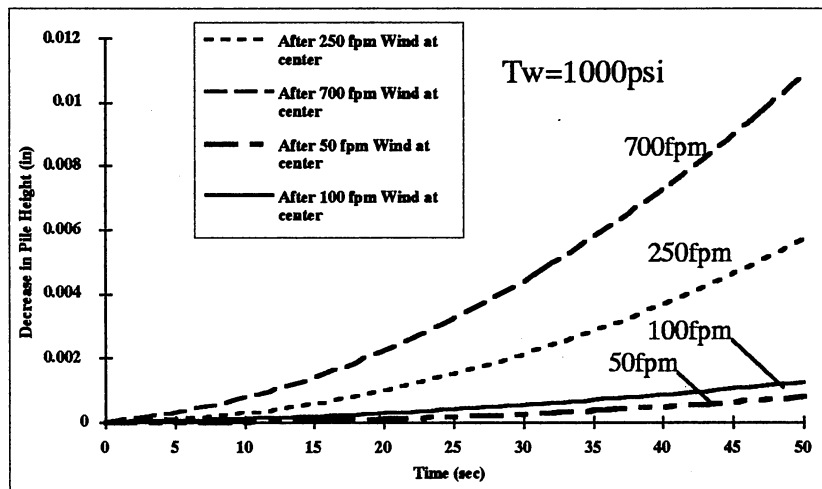


Figure 25. Depletion Data for all Velocities

outcome of the second order regression. Also this type of experimentation shows that after lower velocity winds, less air leakage is found, as shown in Figure 25. One may

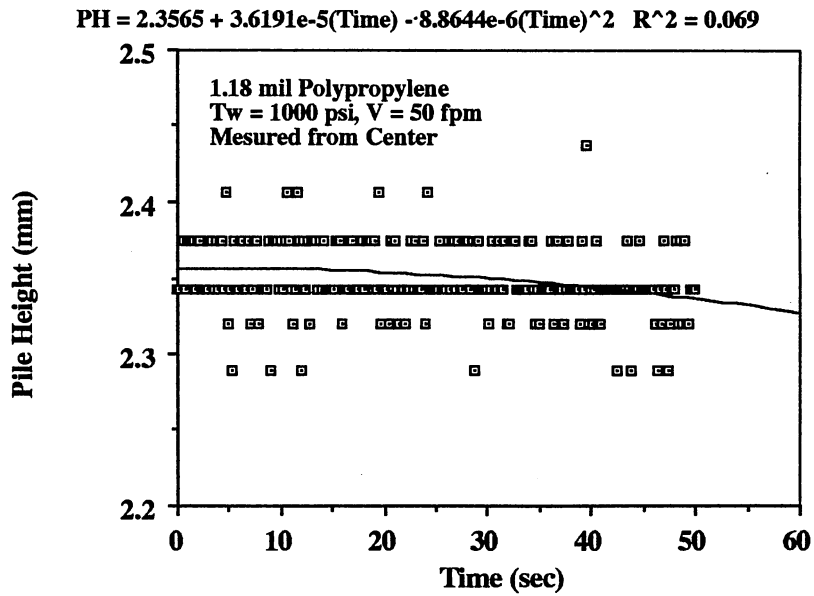


Figure 26. Depletion Regression After a Wind at 50 fpm

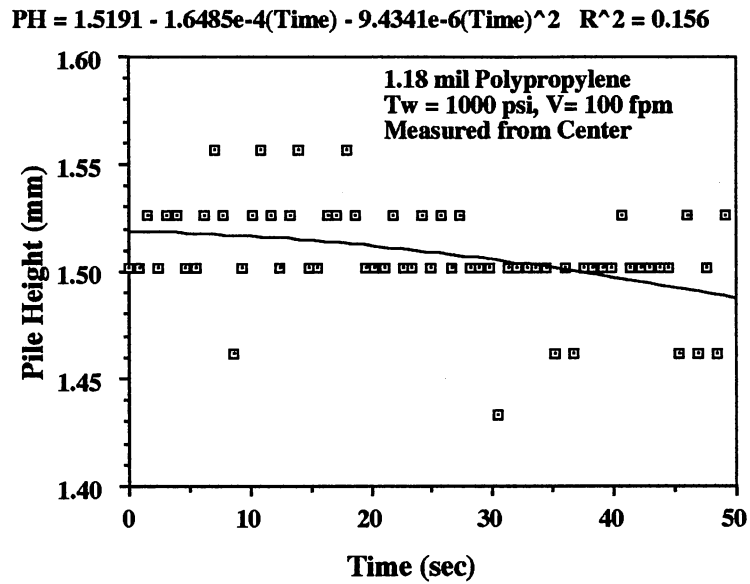


Figure 27. Depletion Regression After a Wind at 100 fpm

question the validity of the second order regression found at lower velocities (50 fpm and 100 fpm). However, this poor regression further proves less air is lost after low velocity

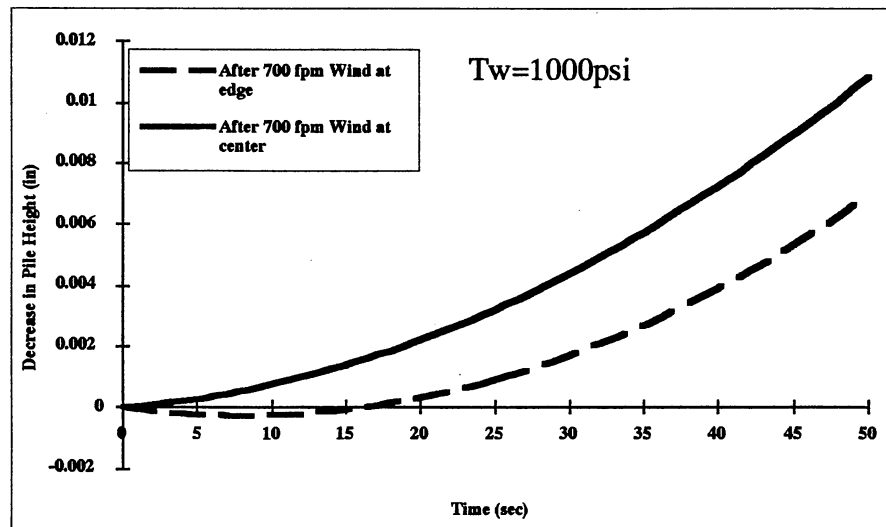


Figure 28. Depletion Comparison at Center and Edge at 700 fpm

winds (see Figures 26 and 27). By applying the same testing procedure simultaneously at the edge of the winding roll, correlation data for radial depletion at the center of the roll to that at the edge can be formulated. Figure 28 shows the radial depletion of both the center and edge of the roll after a wind at 700 fpm. Again, further experimental data are provided in Appendix B for various velocities.

The depletion of the air layer thickness further complicates the entrained air phenomenon. Not only is air being entrained during winding, the entrained air escapes from the roll over a period of time after winding is completed, thus changing the roll structure. The negative values for 0-15 seconds at the edge are due to the edge being slightly inflated as the center of the web depletes, forcing air out at the edge.

Comparison of Laser Data and Foil Bearing Theory

Is this method accurate for measuring air layer thickness within the wound roll? Considering there exist no analytical means to calculate air layer thickness in a wound roll in literature this question is difficult to answer. However, literature does provide theory on air layer thickness of rollers, *THE AIR FOIL BEARING EQUATION*, and this equation could be compared to the laser experimentation data. Although, one must keep in mind that the air foil bearing equations were developed with no possibility of back flow or flow separation over the roller. These equations assume infinitely wide webs and rollers. In the laser experiments, the webs used were 11.5 inches in width not infinite.

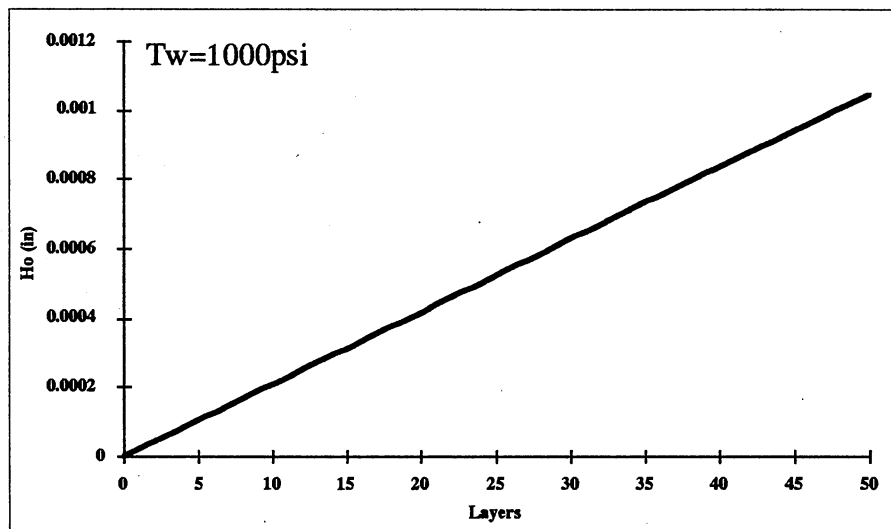


Figure 29. Air Layer Thickness at 50 fpm

These equations do provide a conservative comparison and can dictate the accuracy of the profiles measured.

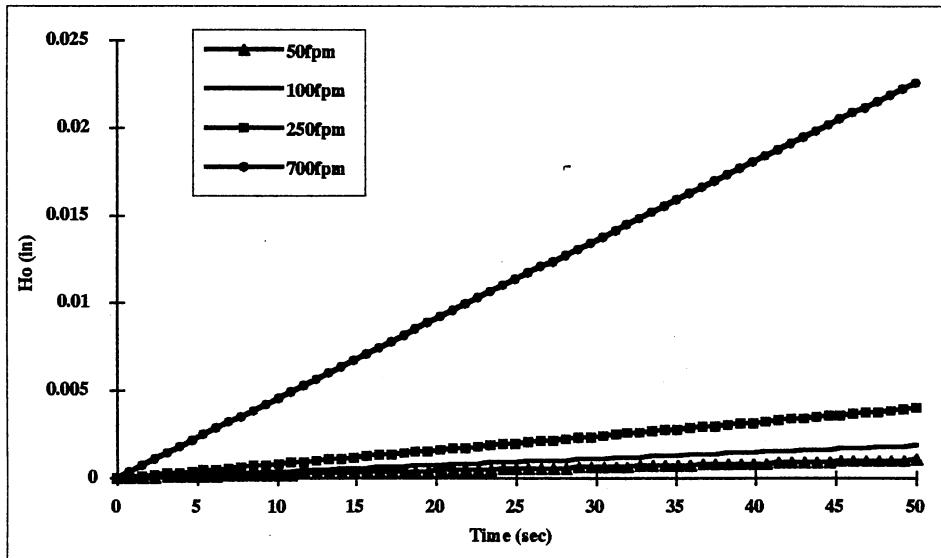


Figure 30. Air Layer Thickness for Various Velocities

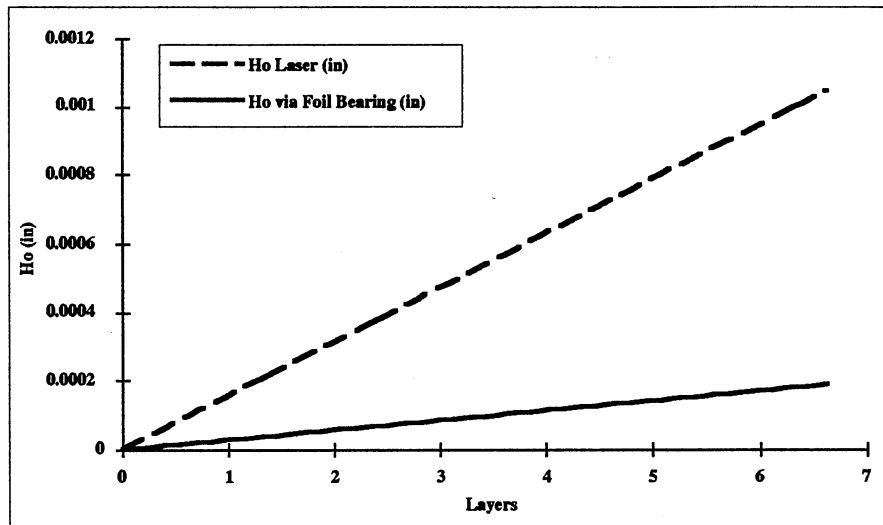


Figure 31. Comparison of Measured and Theoretical Data at 50 fpm

Figure 21 shows pile height as a function of time and, as mentioned earlier,

proves that air is entrained during the wind. However, this figure does not show the air thickness layer by layer. On the contrary, it is showing a sum of air layer thickness and caliper thickness over a period of time. In order to calculate air thickness from the laser data an accurate number of layers must be known over a sample period (sample period was 50 seconds). By assuming that the core radius is sufficiently large, small increases in radius due to incremental web caliper, will not effect the overall radius of the windup roll. Thus, by knowing the number of revolutions for a sample period, one would know the number of layers. Applying this assumption and reasoning to Figure 21, air layer thickness as a function of layers was determined, as shown in Figure 29. Figure 30 provides a representation of air layer thickness for various velocities, demonstrating that with increased velocity there is an increase in air layer thickness.

If the assumption is made that no air is lost as the outer layer is added to the roll, a comparison of the air layer thickness shown in Figure 30 can be compared to values calculated from the air foil bearing equation. Figure 31 provides the comparison of experiment to theory with the assumptions stated earlier. This figure shows that air foil bearing theory is conservative especially at larger radii, however this figure lends promise to using the air foil bearing relationship in the centerwinding configuration, as a conservative description of the air layer thickness.

CHAPTER VI

EXPERIMENTAL DETECTION OF ROLL BODY SLIPPAGE

How the entrained air within a wound roll effects the roll body is still unknown. Does the entrained air induce interlayer slippage (roll body slippage) in the wound roll? If not, is the air producing a spongy or soft roll with high levels of radial deformation due to the addition of each layer? This chapter is dedicated to analyzing if there is in fact roll body slippage occurring as a result of entrained air.

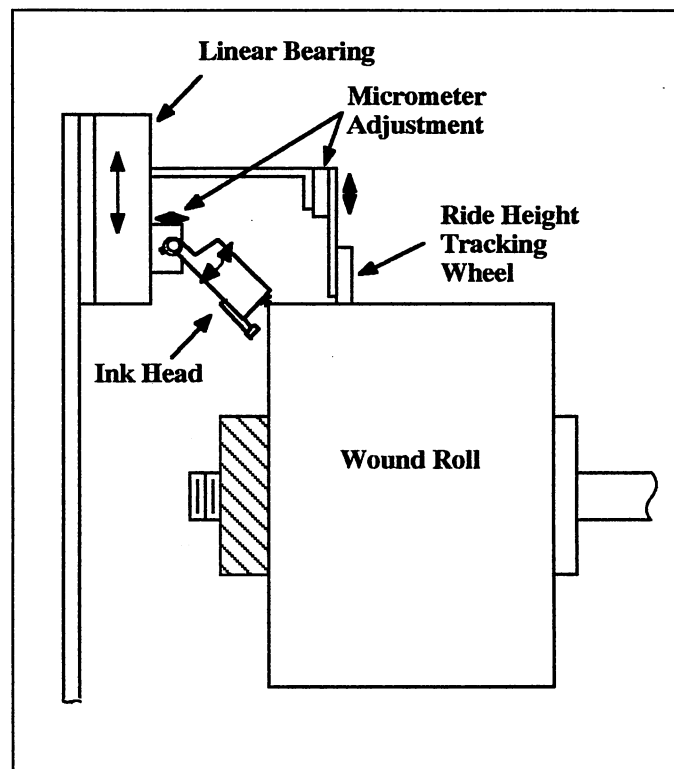


Figure 32. Continuous J-Line Printer

Implementation of the Instantaneous J-Line Printer

The Instantaneous J-Line Printer is a device that was developed in order to visualize if roll body slippage is occurring throughout a wind [3]. This device is simply an ink jet printer head which was fired by a pulse delivered by an encoder fixed to the windup shaft of the 3M Winder Splicer. As the roll is being wound the encoder will send a firing pulse to the ink head which in turn shoots a small line of ink on the edge of the winding roll (see Figure 32). If there exist no interlayer slippage the J-Line Printer will produce a radial line from the core to the outer edge of the roll as shown in Figure 33. However, if roll body slippage is occurring then a skewed line or even a curve line may result as shown in Figure 34.

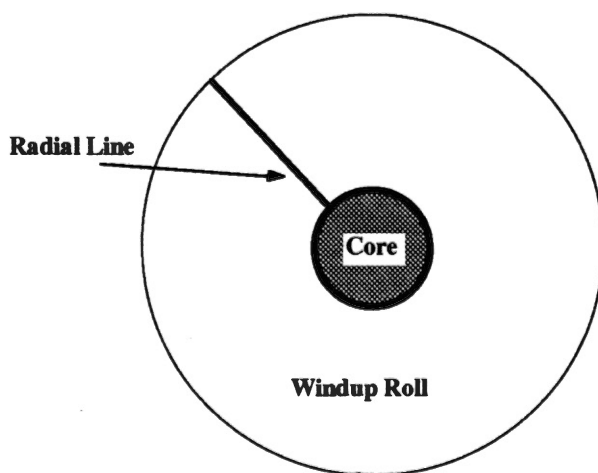


Figure 33. Radial Line Indicating No Roll Body Slippage

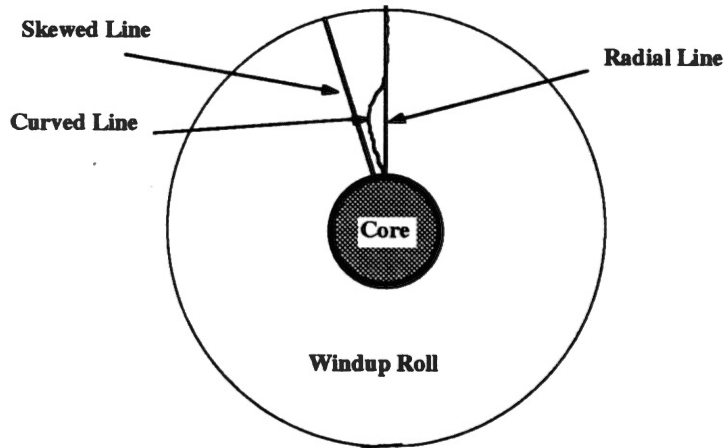


Figure 34. Lines Indicating Roll Body Slippage

Experimental Outcomes

Shown in Figures 35 and 36 is the output of the J-Line experimentation for 92 gage polyester and 2.51 mil newsprint. In these tests, web tension was held constant at 1000 psi while velocity was varied from 50 fpm to 250 fpm and finally back to 50 fpm. These figures show a radial line from the core to the outer edge, proving that with increased velocity there is no roll body slippage. The newsprint was wound to provide a reference to a wind with essentially no entrained air. The step change in velocity for the polyester wind produced a slight telescoping of the web due to the increased entrained air. However, this increase of air entrapment does not effect the output of the J-Line Printer (the radial line). Furthermore, these figures indicate that the interlayer pressure loss must result solely from radial deformation of the wound roll.

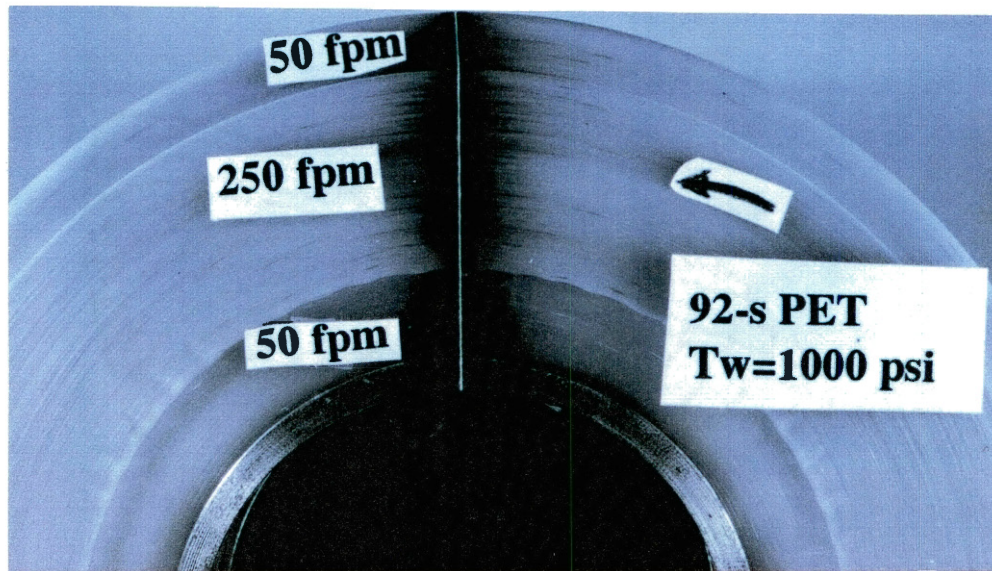


Figure 35. J-Line Output for 92 gage PET

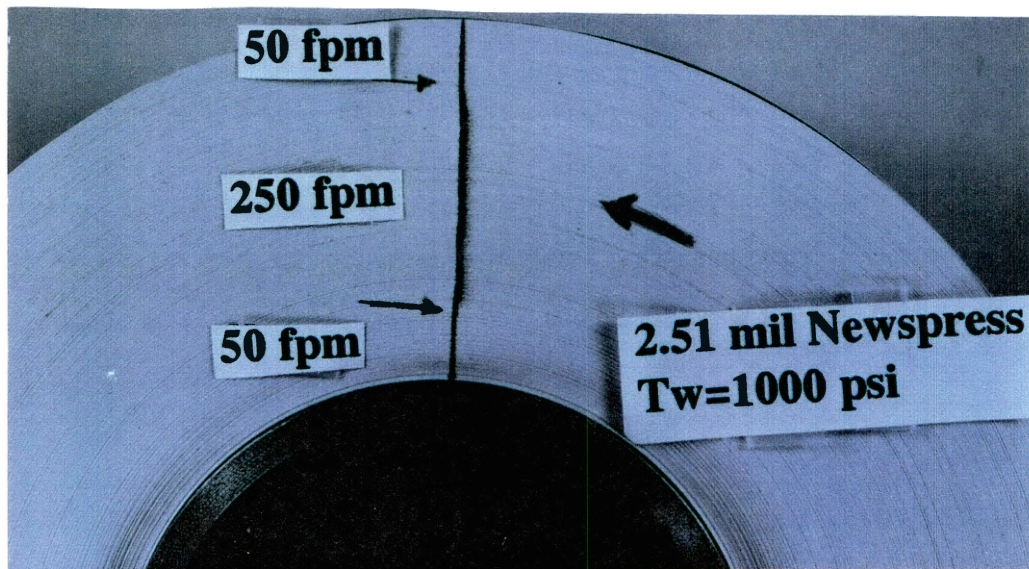


Figure 36. J-Line Output for 2.51 mil Newsprint

CHAPTER VII

DETERMINING AIR INFLUENCED RADIAL MODULUS

The previous chapters have shown that air layer thickness is a function of velocity. Also, tension loss in the outer layer due to entrained air is prevalent. Furthermore, air layer thickness does not induce roll body slippage. However, these results alone cannot account for the large discrepancies realized between existing winding codes and experimental radial pressure data. As foreshadowed in chapter 4 this chapter is devoted to the explanation of the remaining error through the use of a dynamic value of radial modulus (E_r).

Modified Stack Test

In chapter 4 Hakiel's model was run with a static value of E_r . The stack of web material was not rifled, on the contrary the stack was rung together. Therefore, there was no air layer between individual layers. Recalling how E_r is formulated from a stress strain relationship, one may acknowledge how an air layer between layers of web will influence the value of radial modulus. Increasing amounts of air will result in more strain for a given stress. By rifling the stack one is separating the peaks and valleys of adjacent layers, which is what happens when air is entrained in the wound roll. As discussed later in this chapter, with increasing velocities the layers of web can completely float on air. Therefore, rifling the stack can only be compared to low winding velocities. With this in mind a fluffed stack test was performed. By rifling the individual layers of the stack a small air layer was obtained within the stack. Then by following the stack test

procedures outlined in chapter 4 new radial modulus polynomials were obtained. Figures 37, 38 and 39 show the new relationships for radial modulus with a fluffed stack. Figures 40, 41, 42 provide comparisons to Hakiel's model with the fluffed stack test to that of the Hakiel's with static test and experimental data. All of these Figures provide the same conclusion, even at very low winding speeds air is being entrained within the roll and a static E_r is insufficient in describing the E_r of a wound up roll of nonpermeable material with entrained air. However, at higher velocities the large discrepancies between theory and experiment still exist. Therefore, a E_r based on winding speed and air layer thickness must be determined.

Applying Boyle's Law to the Wound Roll

To determine a radial modulus as a function of air layer thickness, a radial modulus for air between the layers must be determined. If one applies Boyle's law,

$$h_o(P_o + P_a) = (P + P_a)h_1 \quad (30)$$

where,

h_1 = final gap distance between layers

h_o = initial air layer thickness

P_a = atmospheric pressure

P_o = initial pressure between layers

P = applied pressure required to compress the air from h_o to h_1

to a single sandwich of web material and air layer, as shown in Figure 43, a E_r for the air may be determined as follows:

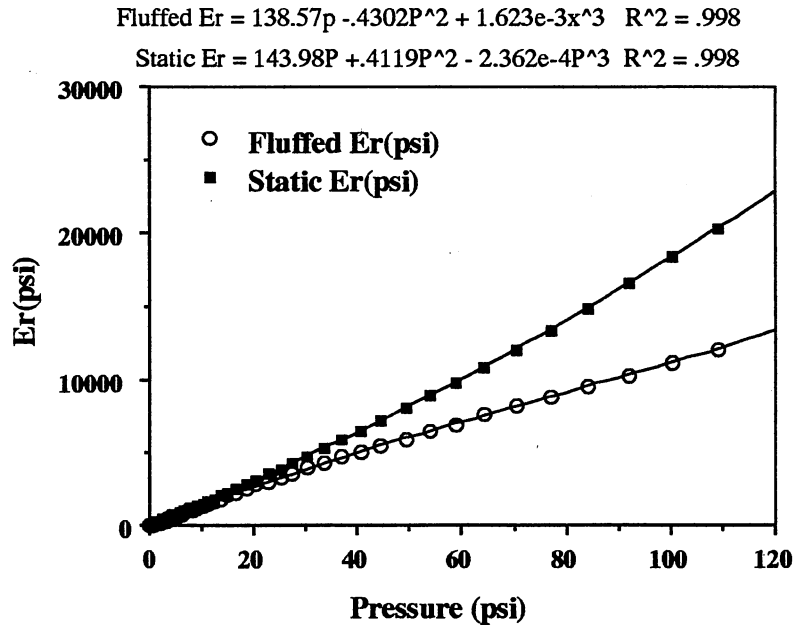


Figure 37. Radial Modulus Profile via Fluffed Stack Test for ICI 48-S PET

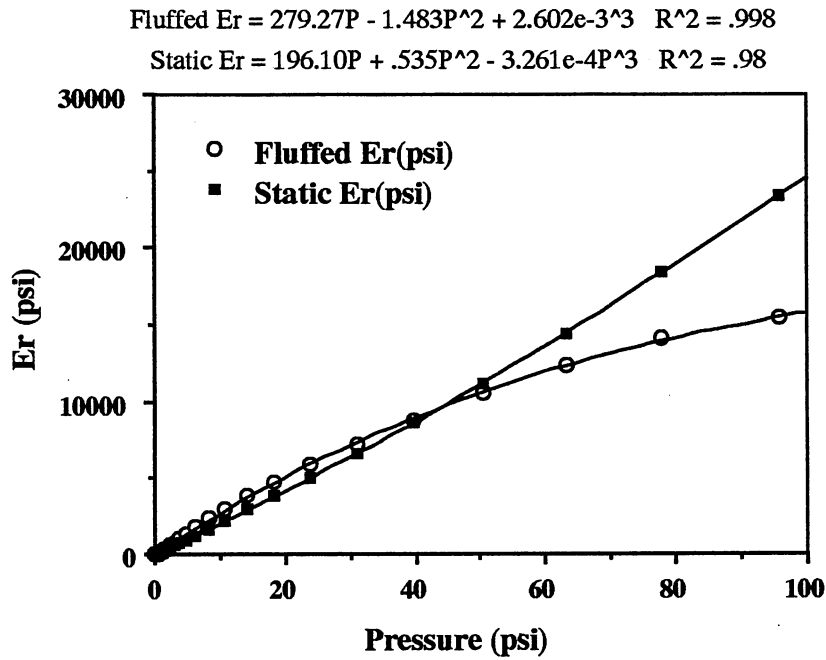


Figure 38. Radial Modulus Profile via Fluffed Stack Test for ICI 92-S PET

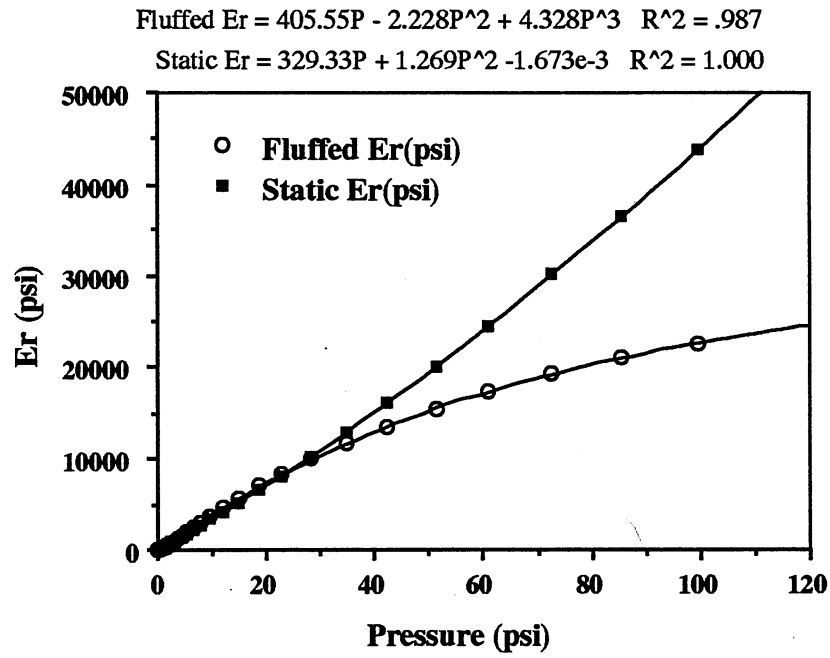


Figure 39. Radial Modulus Profile via Fluffed Stack Test for ICI 200-S PET

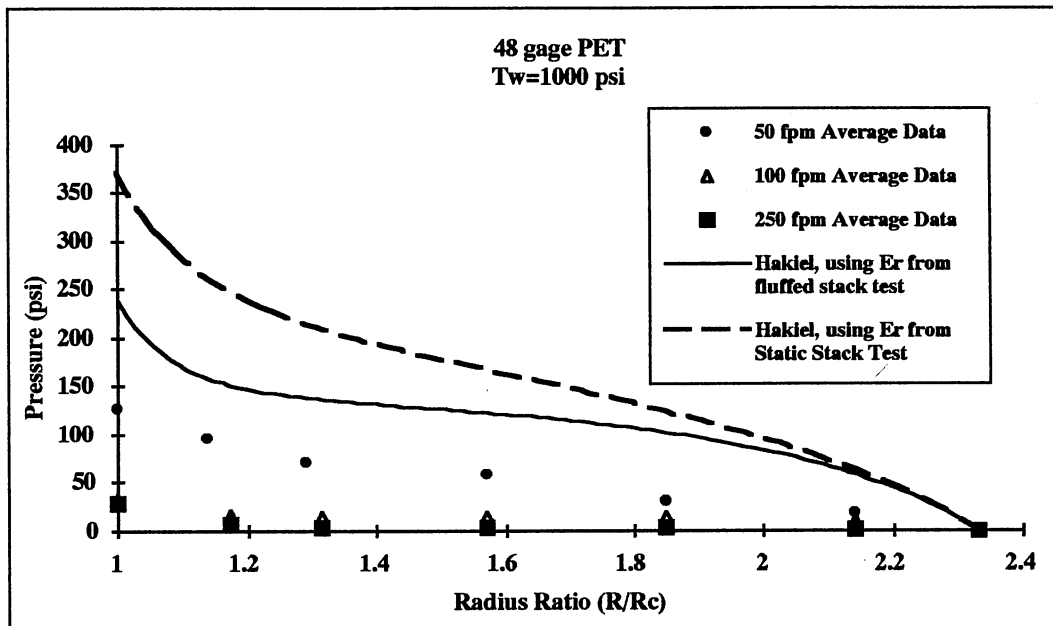


Figure 40. Radial Pressure Profile Comparisons for ICI 48-S PET

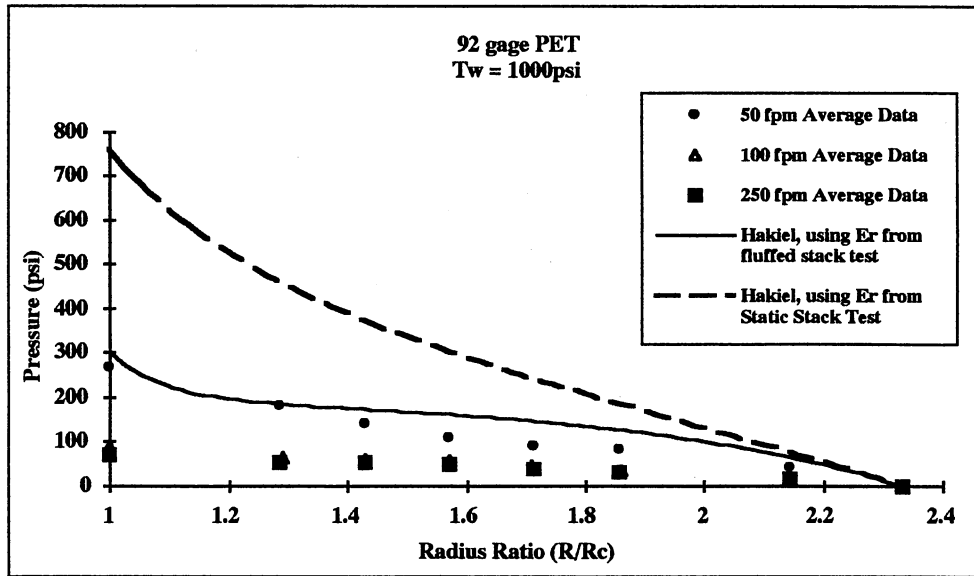


Figure 41. Radial Pressure Profile Comparisons for ICI 92-S PET

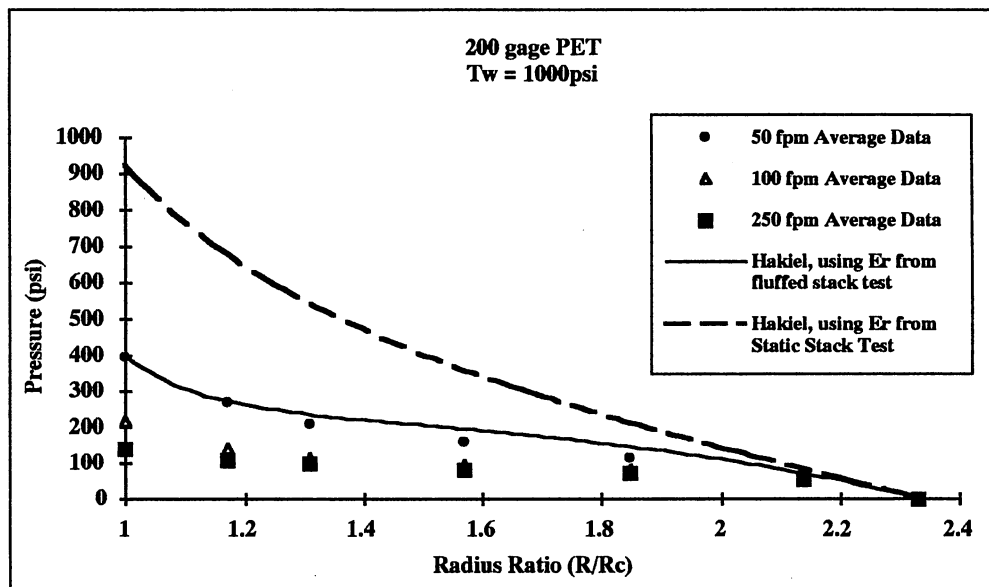


Figure 42. Radial Pressure Profile Comparisons for ICI 200-S PET

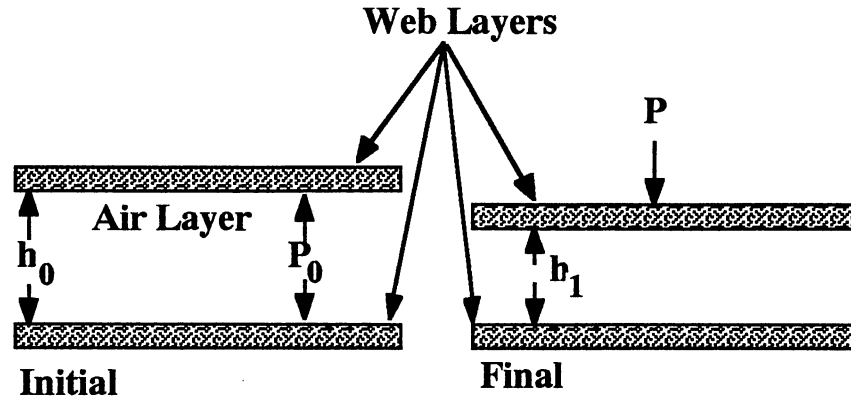


Figure 43. Air Layer Configuration for Boyle's Law

$$h_1 = \frac{(P_0 + P_a)h_0}{(P + P_a)} \quad (31)$$

and now differentiating with respect to pressure,

$$\frac{\partial h_1}{\partial P} = -\frac{(P_0 + P_a)h_0}{(P + P_a)^2} \quad (32)$$

and finally assuming compressive pressure is a positive number, dividing both sides by h_0 , and multiplying by a surface area per unit width (A), a radial stiffness for the air layer is determined:

$$K_{\text{air}} = \frac{(P_0 + P_a)^2 A}{h_0(P + P_a)} \quad (33)$$

This value depends upon the air layer thickness (h_0). Recalling from chapter 5, the foil

bearing equation was determined to be a conservative estimate of air layer thickness in a wound roll. Therefore, conservative values of air layer thickness as a function of velocity and web thickness can be determined. Allowing a varying radial moduli for increasing amounts of entrained air. However, this value does not include the modulus of the web material. The modulus determined for the stack must be added to evaluate an E_r for a wound roll containing air. It is assumed that the stiffness of the stack and the entrained air behaves like springs in series. The following relationships provides the equation for determining the total E_r in a roll containing air.

$$\frac{1}{K_{eq}} = \frac{1}{K_{stack}} + \frac{1}{K_{air}} \quad (34)$$

$$K_{air} = \frac{(P_0 + P_a)^2 A}{h_0(P + P_a)} \quad (35)$$

and for the stack,

$$K_{stack} = \frac{E_r A}{h} \quad (36)$$

where h is the web caliper,

$$K_{eq} = \frac{E_{r,total} A}{h + h_0} \quad (37)$$

solving for E_r , total yields,

$$E_{r,total} = \frac{h + h_0}{\frac{h}{E_{r,stack}} + \frac{h_0(P_0 + P_a)}{(P + P_a)^2}} \quad (38)$$

TABLE 1

RADIAL MODULUS POLYNOMIAL COEFFICIENTS
INCLUDING AIR ENTRAINMENT

General Equation $E_r = C1*P + C2*P^2 + C3*P^3$

Material	C1	C2	C3	R²
48 gage PET				
50fpm	13.851	0.1309	3.235E-03	0.9994
100fpm	10.259	0.0972	3.399E-04	0.9993
250fpm	7.306	0.0682	3.140E-04	0.9991
92 gage PET				
50fpm	37.9241	0.1243	1.751E-03	0.9991
100fpm	26.5646	0.0674	1.826E-03	0.9988
250fpm	16.9671	0.0246	1.571E-03	0.9984
200 gage PET				
50fpm	111.705	1.0818	-6.143E-03	0.9998
100fpm	77.285	1.0122	-4.319E-03	0.9996
250fpm	46.336	0.7367	-1.777E-03	0.9995

Now new radial modulus polynomials as functions of pressure may be determined for the three gages of polyester used in experimental winding at velocities of 50, 100, 250 fpm. Table 1 provides the coefficients of the curve fits for all materials at all velocities.

Comparisons of Theory and Experiment

By inputting these new radial moduli into Hakiel's model, new interlayer pressure profiles which are shown in Figures 44,45, and 46. The model predicts the radial pressures at 100 and 250 fpm quite well. At 50 fpm the model yielded pressures which were much too low. An explanation was sought by studying surface roughness data for the three calipers of polyester to determine at what radius location fully entrained air layer status is reached. By applying the foil bearing equation to radius at the core (1.75 in) and at the outer edge of the roll (4.08 in), a air layer thickness range was determined for all experimental velocities, Figures 48-50 show these comparisons. The surface roughness data taken by WYKO Surface Interferometer, was provided by ICI Films. The mean surface roughness data was determined from the average of 10 separate measurements of peaks above 1000 nanometers (nm), then the data was converted to English units.

These comparisons provide insight to the results of Figures 44-46. For instance in Figure 48 the air layer is not fully developed until approximately 3.5 in at 50 fpm, which proves why the predicted curve shown in Figure 47 does not converge with experimental data until 1.85 roll radius ratio. Furthermore, the same holds true for 100 fpm case in Figure 46, the point of transition does not occur until 1.14 roll radius ratio. To explain why the measured values that are higher than the predicted cases after transition is reached one can recall the depletion data provided in chapter 5. Air can be entrained in the wound roll only if it is being wound in more rapidly than it is escaping out of the roll edges and the entry point, if recirculation is occurring. Figures 25, 26 and 27 illustrate this point. This reason could be the source of the larger differences between theory and experiment at 50 fpm for all materials. At 50 fpm, the air layer being entrained is not very significant and can escape more rapidly than larger air layers. Figure 46 represents this phenomena at 250 fpm, the experimental interlayer pressures follow the profile of the predicted curve, however they lie slightly above. Figure 45 also supports this idea at

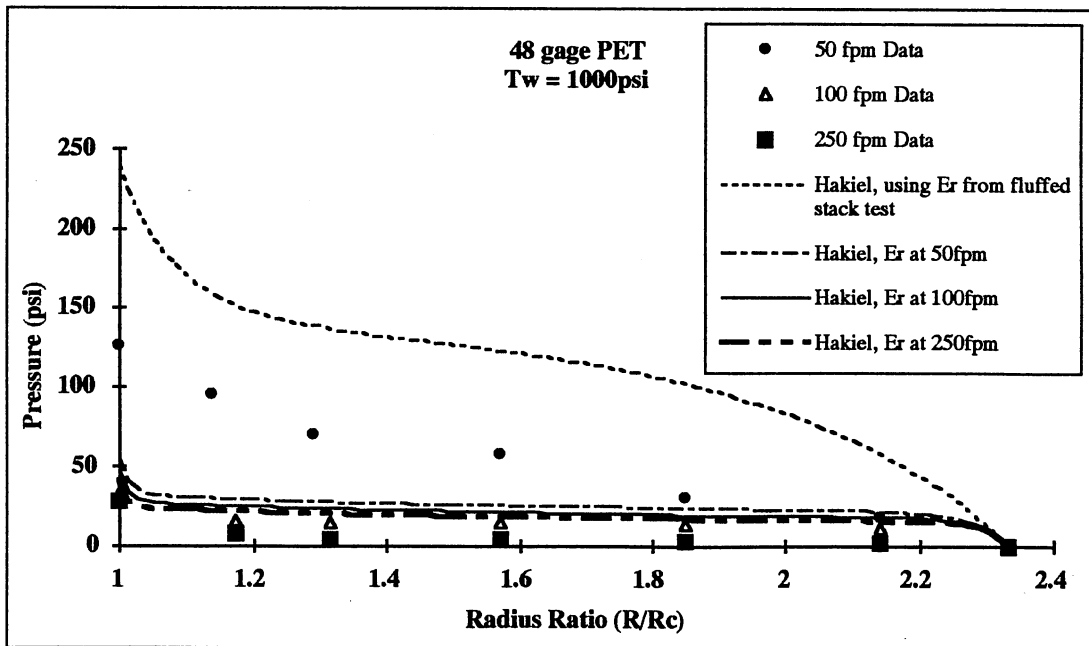


Figure 44. Radial Pressure Profile Comparisons for ICI 48-S PET

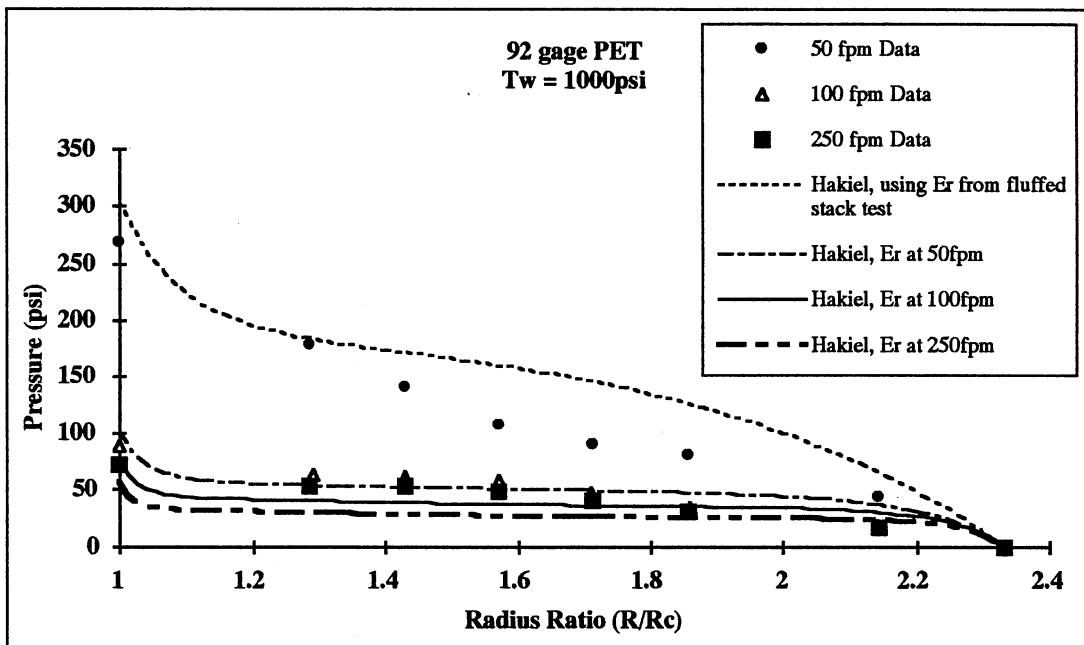


Figure 45. Radial Pressure Profile Comparisons for ICI 92-S PET

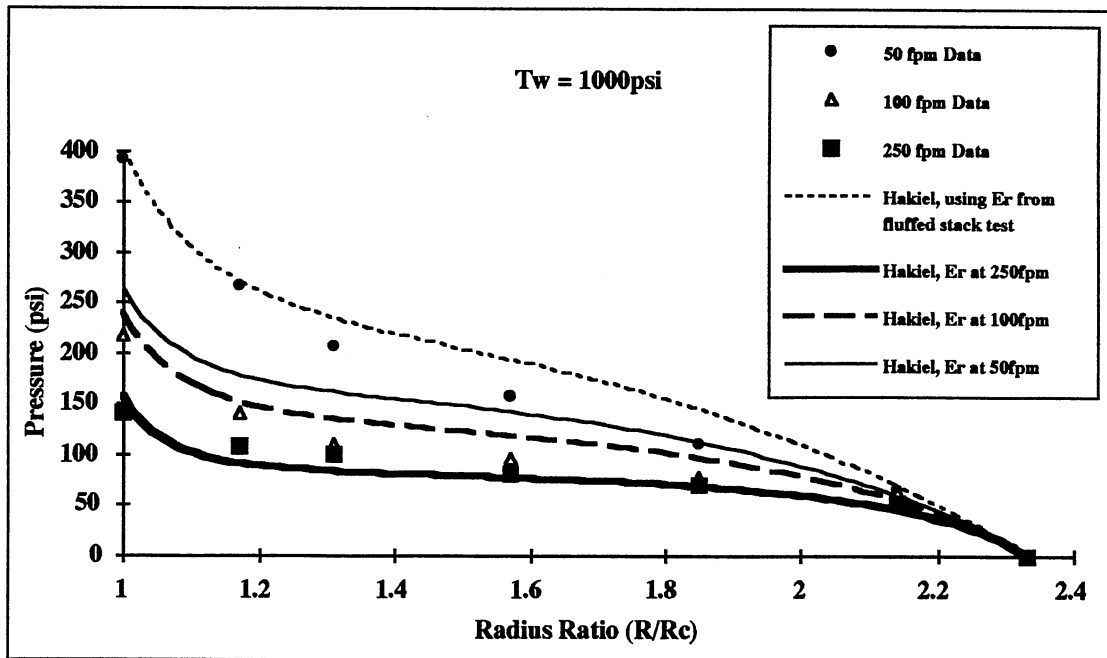


Figure 46. Radial Pressure Profile Comparisons for ICI 200-S PET

100 and 250 fpm values of radial pressure actually increase slightly over an increase in roll radius. Moreover, the bar graphs provide reasoning as to why the fluffed stack test provides good correlation at 50 fpm in Figures 45 and 46. Since the air layer is small during a 50 fpm wind one is able to fluff a stack of web sufficiently to model this low winding velocity case. Lastly, Figure 45 shows that the new E_r is a conservative value due to the conservative nature of applying the foil bearing equation to the geometry of the wound roll. This is noticed by the lower measured interlayer pressures measured at 100 and 250 fpm. This method does provide generally good correlation for velocities at which the totally entrained status has been reached.

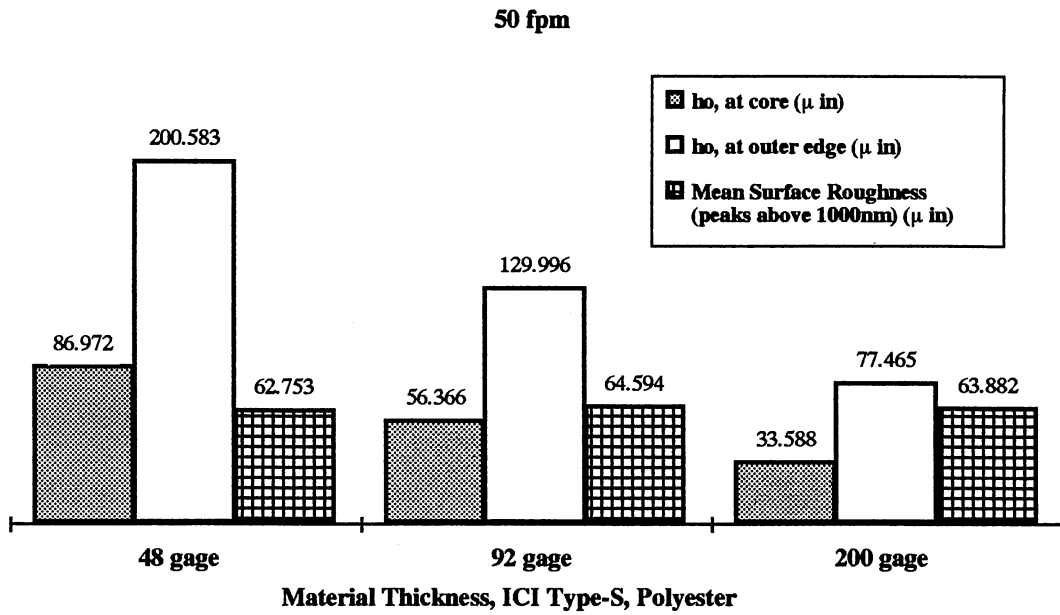


Figure 47. Air Layer Thickness and Surface Roughness at 50fpm

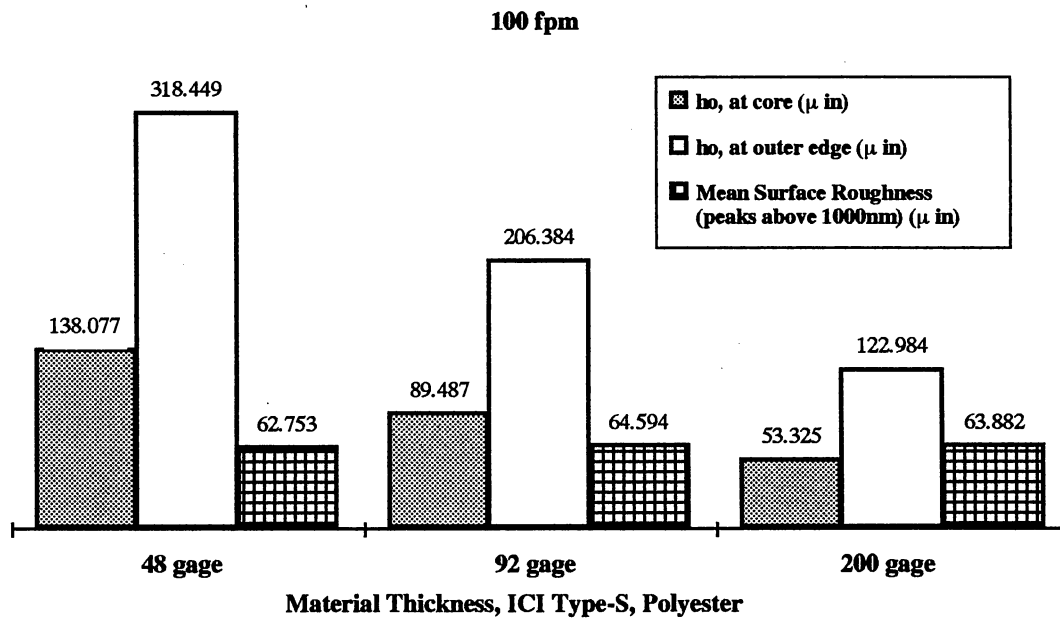


Figure 48. Air Layer Thickness and Surface Roughness at 100fpm

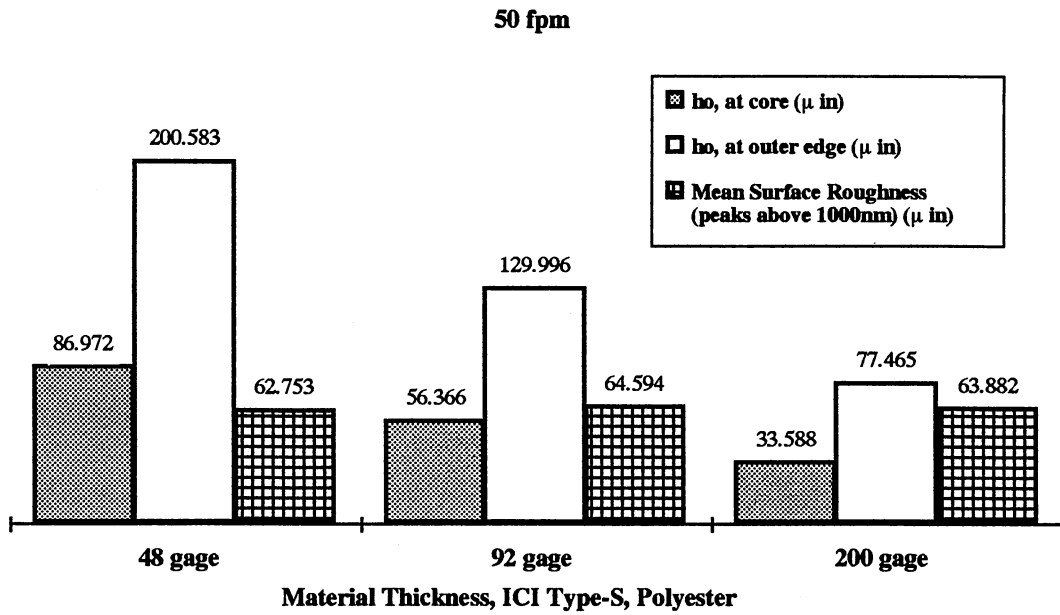


Figure 47. Air Layer Thickness and Surface Roughness at 50fpm

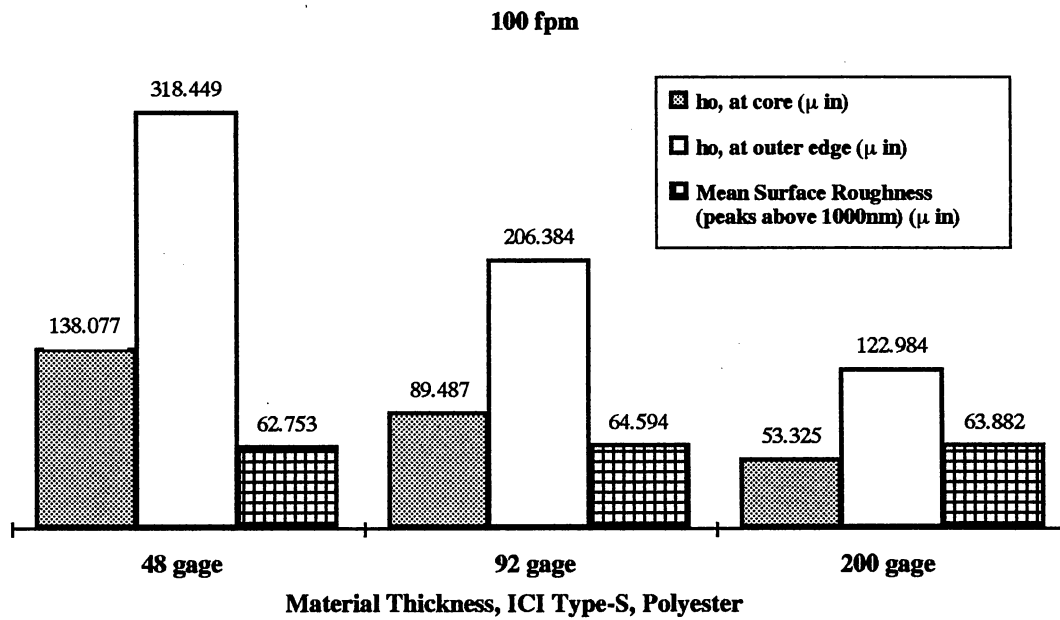


Figure 48. Air Layer Thickness and Surface Roughness at 100fpm

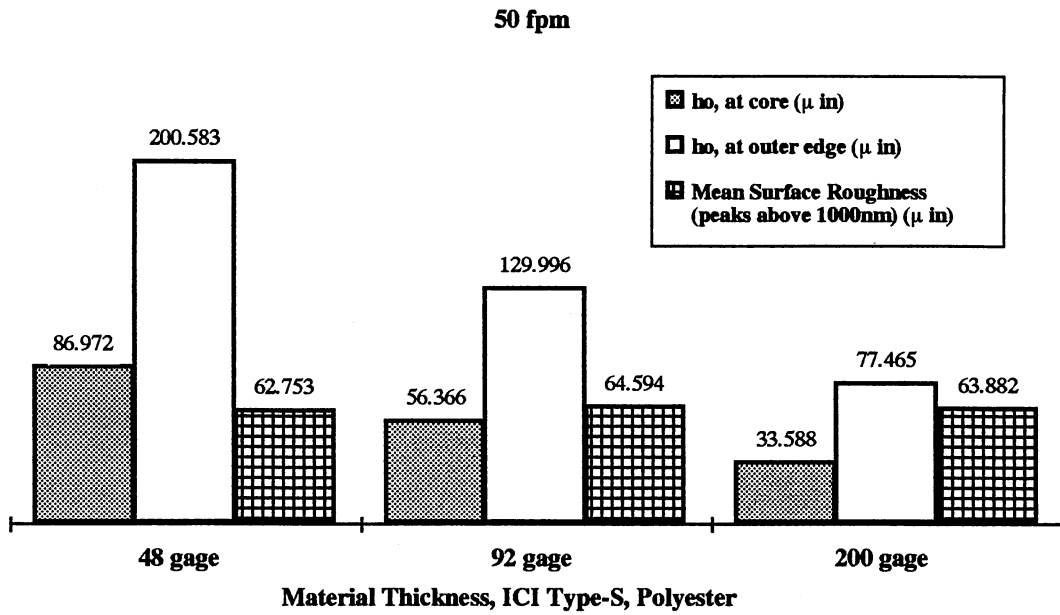


Figure 47. Air Layer Thickness and Surface Roughness at 50fpm

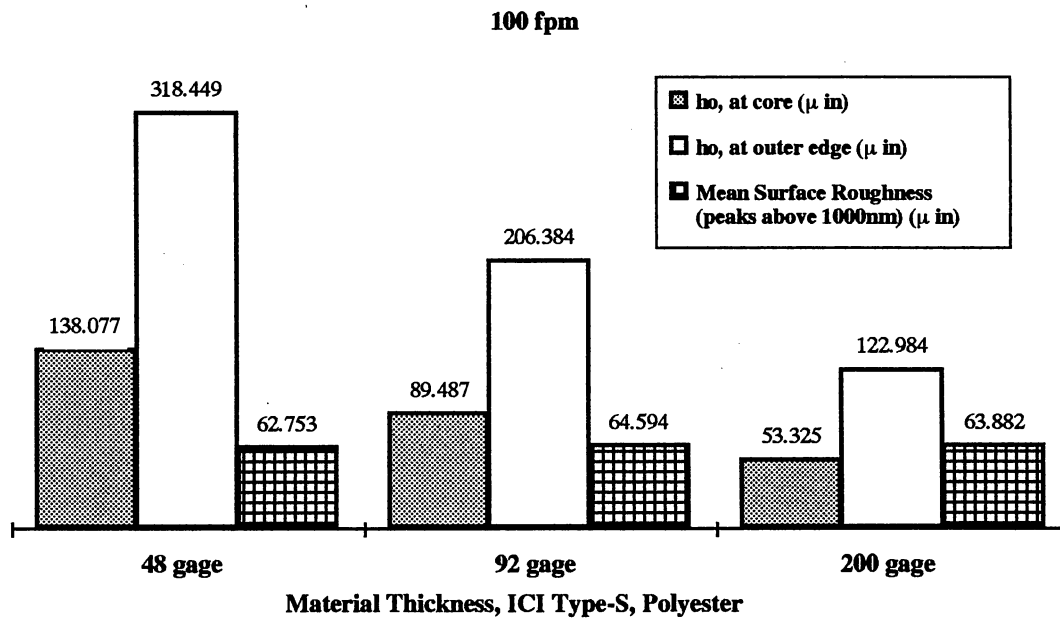


Figure 48. Air Layer Thickness and Surface Roughness at 100fpm

- 3.) Hakiel's Model can be used to predict the radial pressure in wound rolls with entrained air, with modifications of the radial modulus.

Future Research

The results of this research are promising, they provide insight to little known phenomenon of air entrainment in wound rolls. However, this research does fall short of explaining all aspects of air entrainment in wound rolls. Various areas could be studied to provide a more broad understanding of this aspect of winding including:

1. Caliper variations within the web material, and static electricity were not considered in this work. However, material defects such as this could alter the results of this research.
2. Radial modulus data were found to be a function of air layer thickness therefore the radial modulus of a wound roll may also be a function of time or atmospheric conditions. These areas should be analyzed to determine their effects on the wound roll.
3. Further experimental data should be analyzed to provide a better acceptance of the results found in this work. Equipment limitations did not allow the analysis of high winding speeds, at higher winding speeds entrained air becomes a problem in handling the wound roll.
4. Air layer depletion needs further research. With increasing amounts of time does the air layer completely vanish, allowing the roll to be analyzed as an homogeneous solid? How long after a wind does it take for the roll to reach equilibrium? These questions must be considered to further aid in the understanding of the wound roll.

REFERENCES

1. Altmann, H.C. "Formulas for Computing the Stresses in Center-wound Rolls." Tappi Journal, Volume 51, no.4, pp176-179, April 1968.
2. Eshell, A. and Elrod, JR., H.G. "The Theory of the Infinitely Wide, Perfectly Flexible, Self-Acting Foil Bearing." Journal of Basic Engineering, Trans. ASME, Series D, Volume 87, No. 4, December. 1965, pp. 831-836.
3. Giachetto, R., M. "Tension Losses Encountered in Centerwound Rolls." Masters Thesis, Department of Mechanical and Aerospace Engineering, Oklahoma State University, 1992.
4. Hakiel, Z. "Nonlinear Model for Wound Roll Stresses", Tappi Journal, Volume 70, No. 5, pp. 113 - 117, 1987.
5. H. Blok and J.J. van Rossum, "The Foil Bearing Departure in Hydrodynamic Lubrication." Lubrication. Engineering, Volume 9, December, 1953, pp. 310-320.
6. Fikes, M., "The Use of Force Sensing Resistors to Measure Radial Interlayer Pressures in Wound Rolls." Master Thesis, Department of Mechanical and Aerospace Engineering, Oklahoma State University, 1990.
7. Knox, K.L, Sweeny, "Fluid Effects Associated with Web Handling." Ind. Engr. Chem. Proc., vol. 10, October 1971, pp.201-205.
8. Pfeiffer, J. D. "Internal Pressures in a Wound Roll of Paper", Tappi Journal, Volume 49, No. 8, pp. 342 - 347, 1966.
9. Roisum, D.R. "The Measurement of Web Stresses During Roll Winding." Ph.D Thesis, Department of Mechanical and Aerospace Engineering, Oklahoma State University, 1990.
10. Swanson, R.P., "Determination of Wound Roll Structure Using Acoustic Time of Flight Measurements", Master Thesis, Department of Mechanical and Aerospace Engineering, Oklahoma State University, December 1991.

APPENDICES

APPENDIX A
WINDING EXPERIMENTATION

STATIC RADIAL MODULUS DATA

Presented in this section are data that were generated by the stack test procedures presented in chapter 4.

$$E_r = 143.98P + .41186P^2 - 2.3622e-4P^3 \quad R^2 = 0.998$$

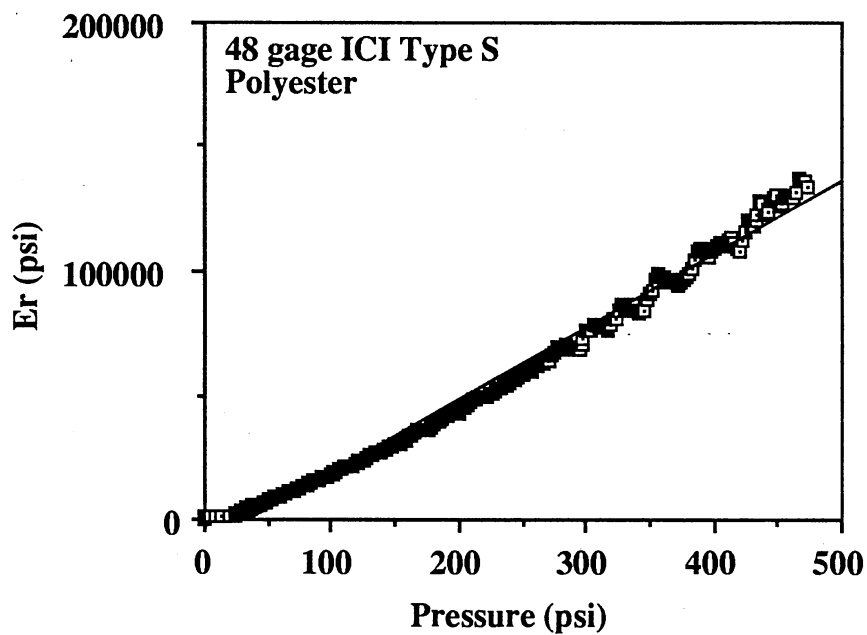


Figure 50. Radial Modulus as Function of Pressure for 48 gage

$$E_r = 196.1P + 0.535P^2 - .000326P^3 \quad R^2 = 0.98$$

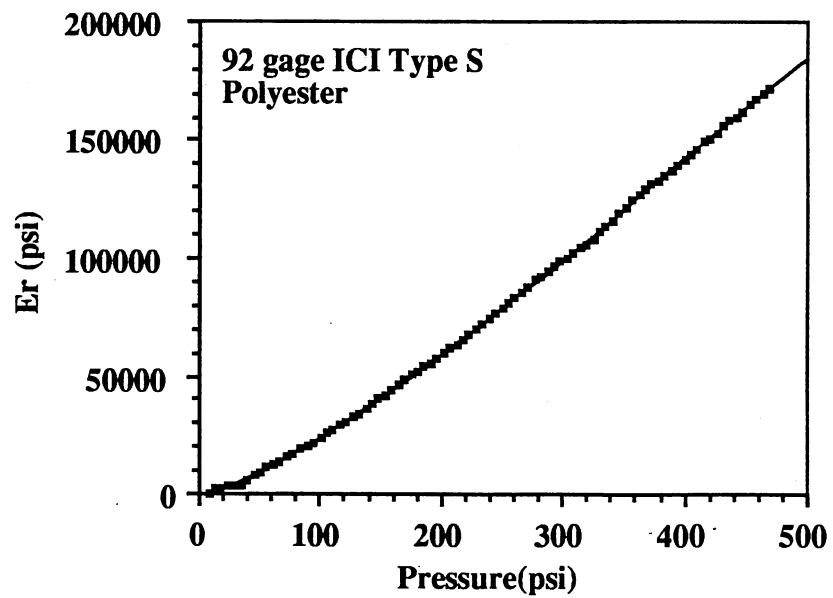


Figure 51. Radial Modulus as Function of Pressure for 92 gage

$$E_r = 329.33P + 1.2685P^2 - 1.6729e-3P^3 \quad R^2 = 1.000$$

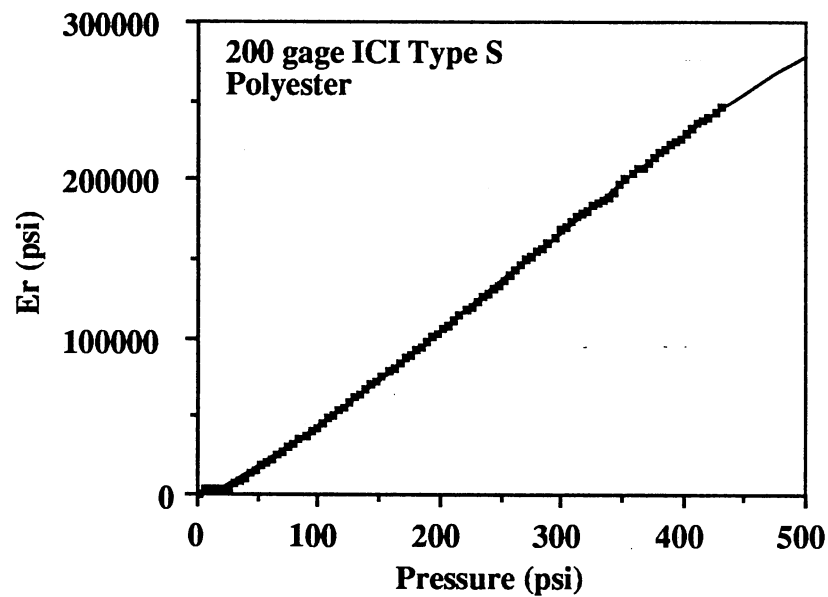


Figure 52. Radial Modulus as Function of Pressure for 200 gage

EXPERIMENTAL DATA FOR INTERLAYER PRESSURE

This Section Presents the experimental data acquired during the empirical winding phase of chapter 4.

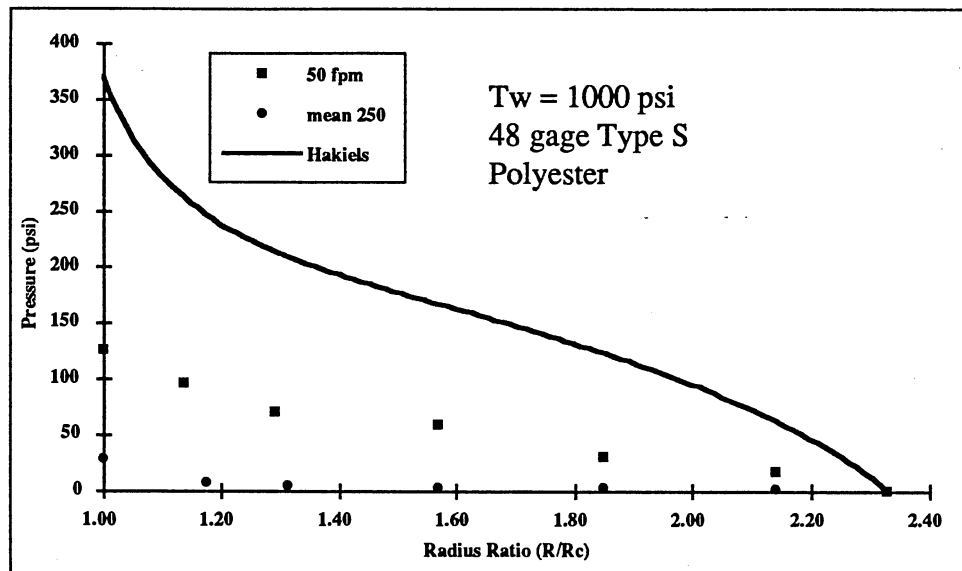


Figure 53. Experimental and Theoretical Radial Pressure Comparison 48 gage

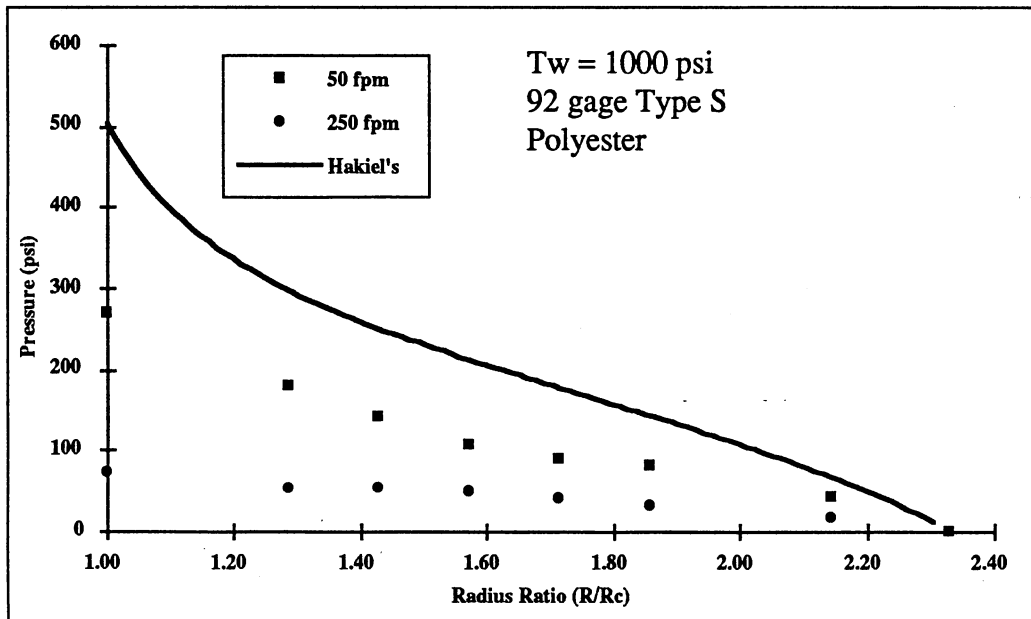


Figure 54. Experimental and Theoretical Radial Pressure Comparison 92 gage

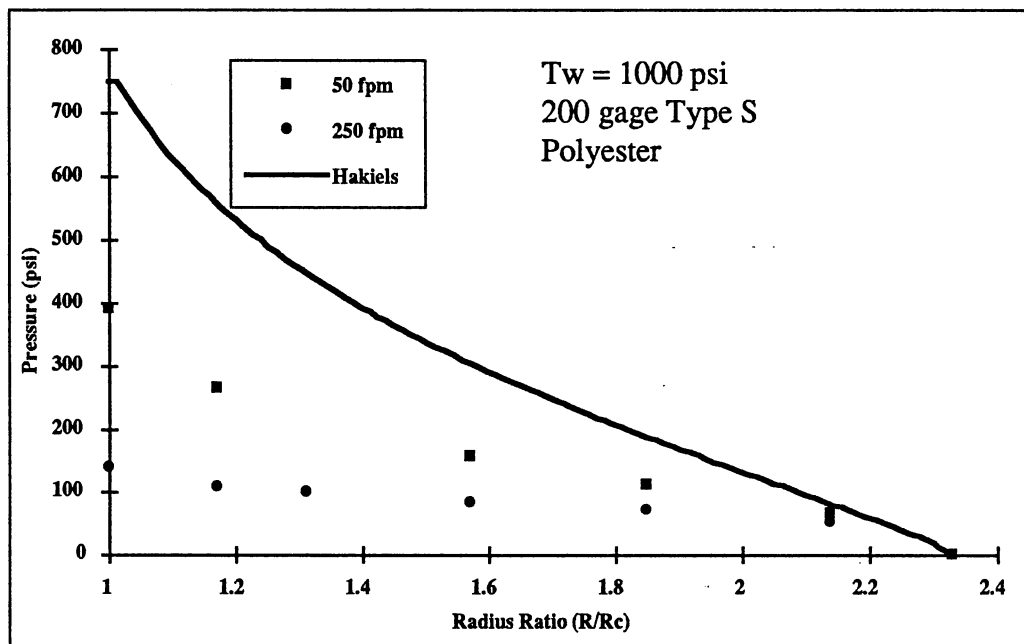


Figure 55. Experimental and Theoretical Radial Pressure Comparison 200 gage

BOUNDARY CONDITION TEST RESULTS

This section provides the experimental results from applying the boundary condition tests explained in chapter 4.

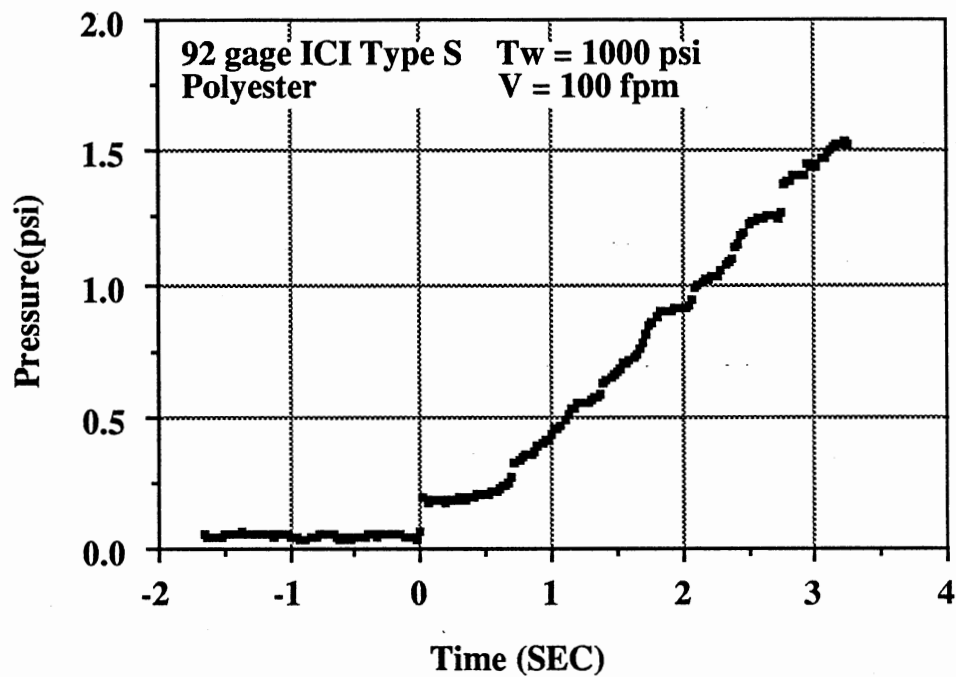


Figure 56. Boundary Condition Test Results at 100 fpm

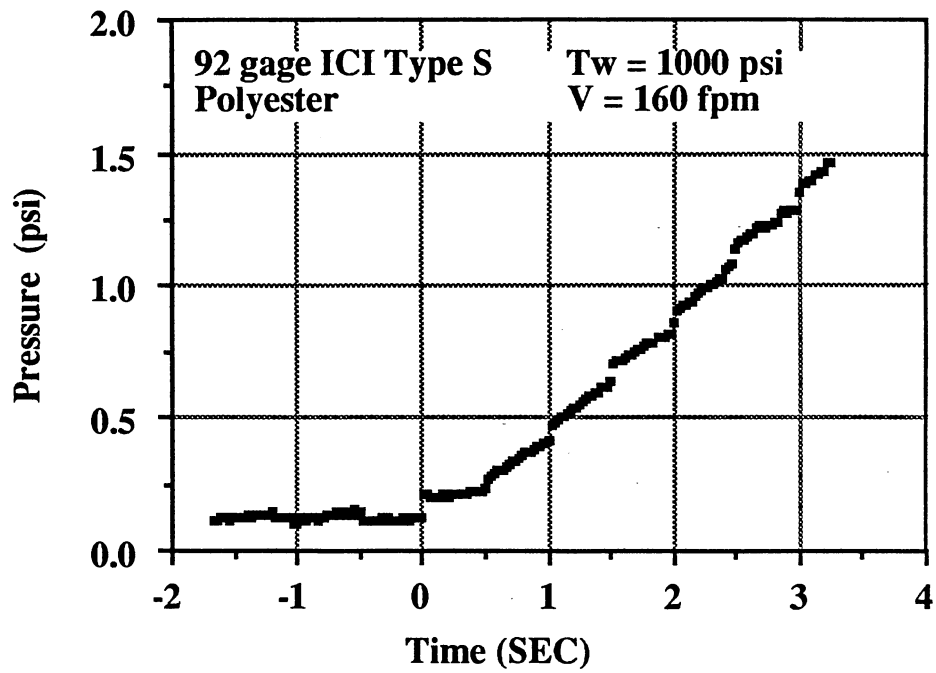


Figure 57. Boundary Condition Test Results at 160 fpm

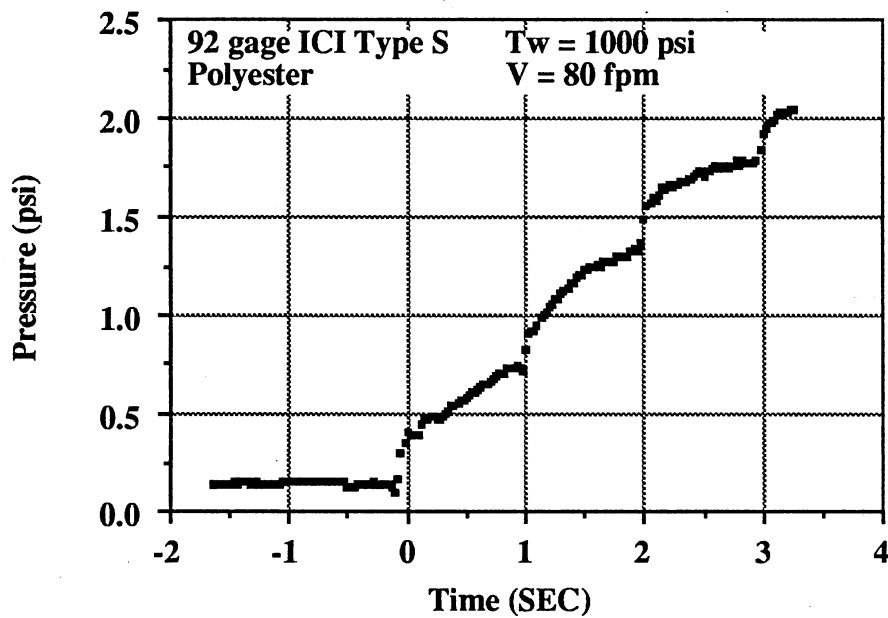


Figure 58. Boundary Condition Test Results at 80 fpm

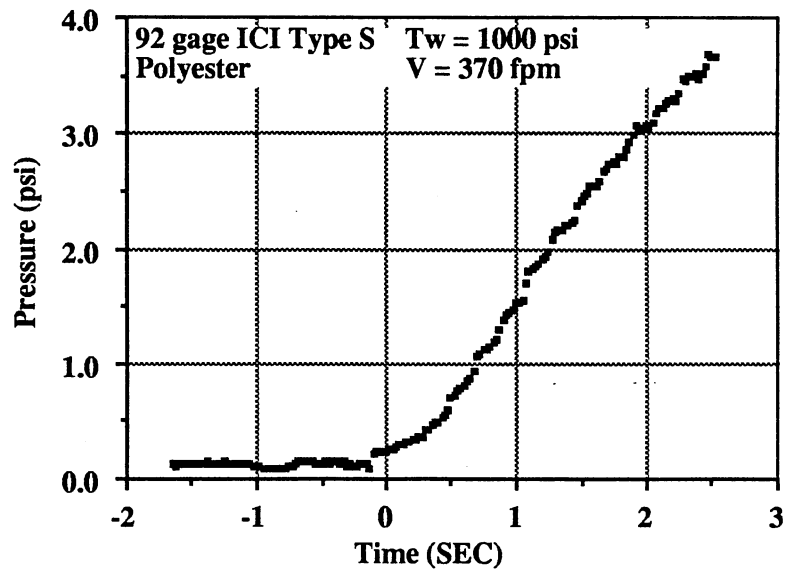


Figure 59. Boundary Condition Test Results at 370 fpm

APPENDIX B

LASER EXPERIMENTATION

AIR LAYER EXPERIMENTAL DATA

Presented in this section are the relative data that were generated from the laser experimentation procedures provided in chapter 5.

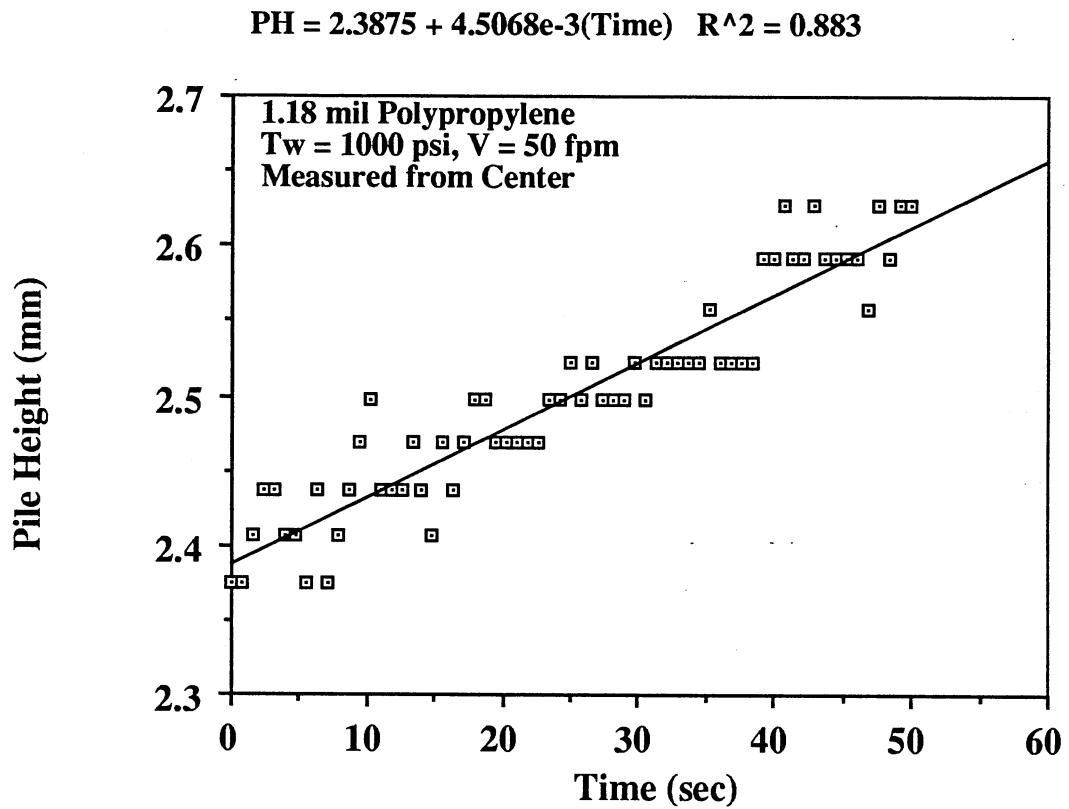


Figure 60. Pile Height Regression for Wind at 50 fpm

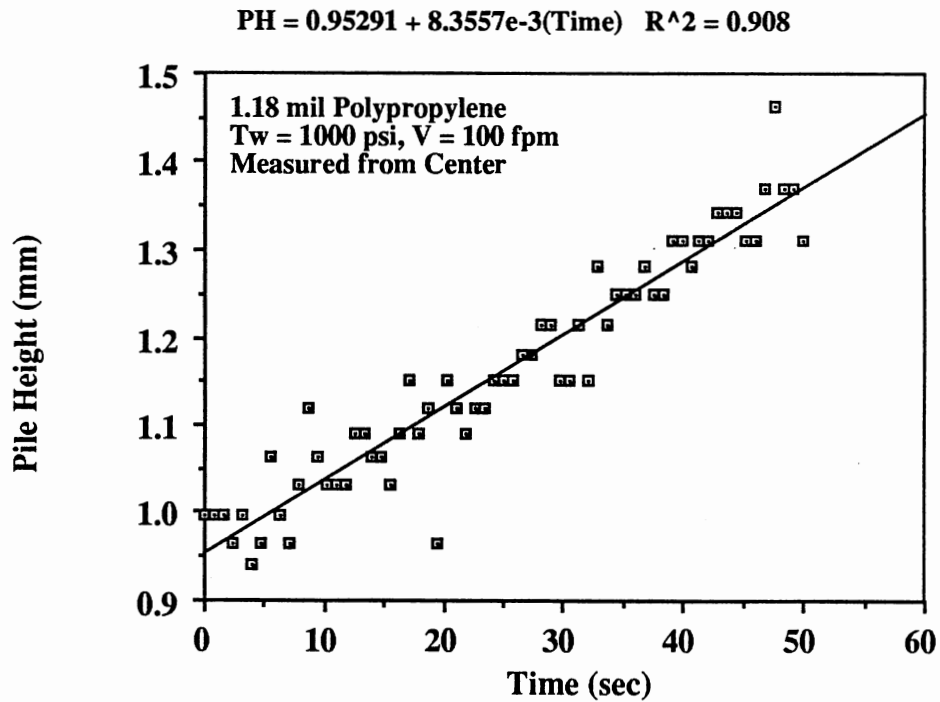


Figure 61. Pile Height Regression for Wind at 100 fpm

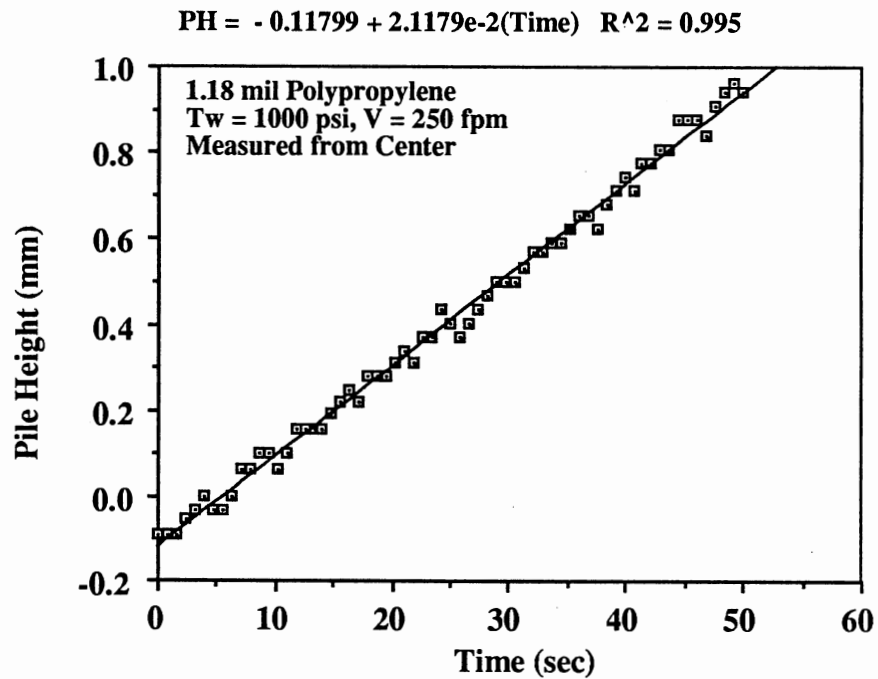


Figure 62. Pile Height Regression for Wind at 250 fpm

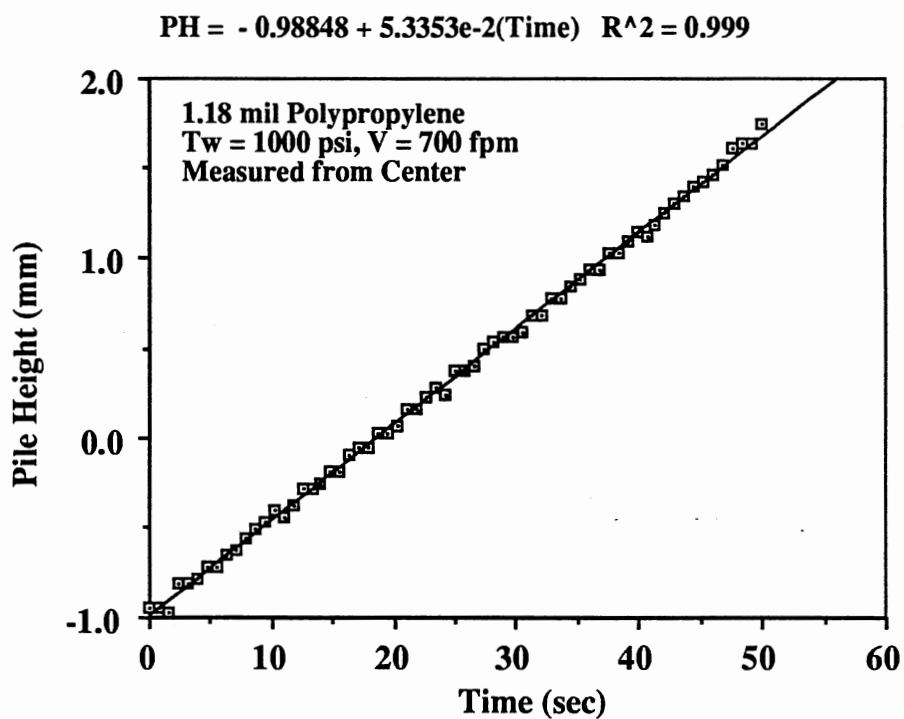


Figure 63. Pile Height Regression for Wind at 700 fpm

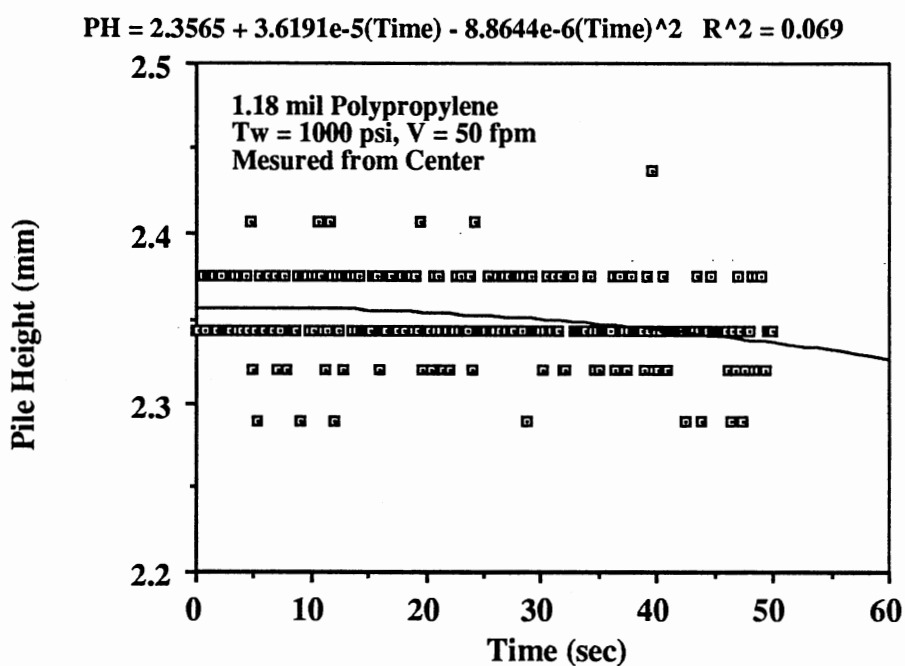


Figure 64. Depletion Regression for Wind at 50 fpm

$$PH = 1.5191 - 1.6485e-4(\text{Time}) - 9.4341e-6(\text{Time})^2 \quad R^2 = 0.156$$

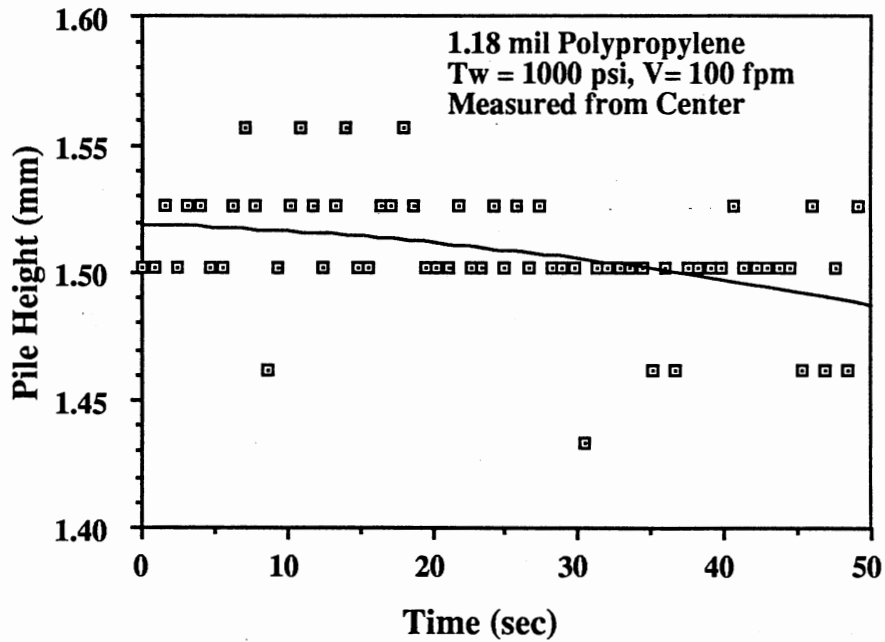


Figure 65. Depletion Regression for Wind at 100 fpm

$$PH = -0.34435 - 1.5825e-4(\text{Time}) - 5.4201e-5(\text{Time})^2 \quad R^2 = 0.799$$

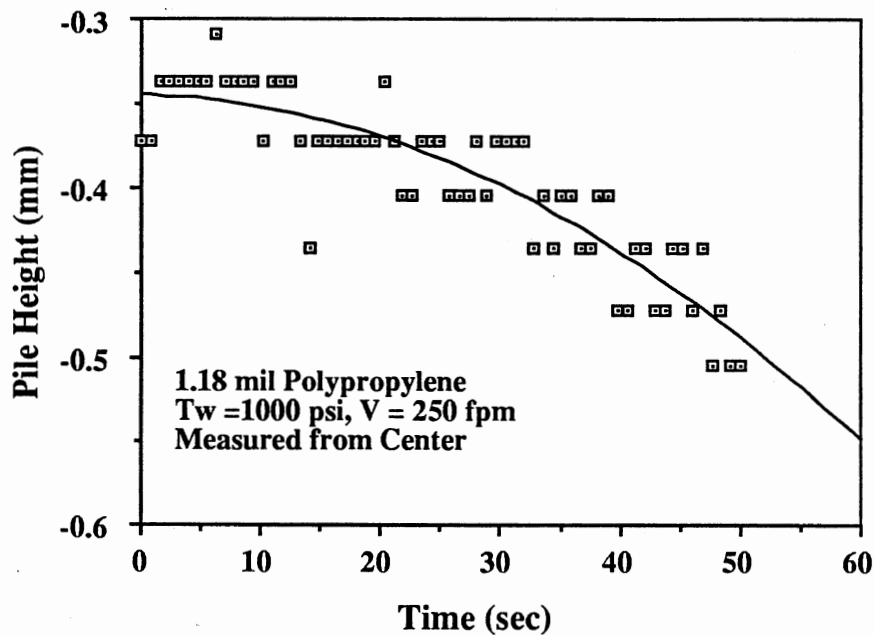


Figure 66. Depletion Regression for Wind at 250 fpm

$$PH = -1.3273 - 1.0263e-3(\text{Time}) - 8.9629e-5(\text{Time})^2 \quad R^2 = 0.935$$

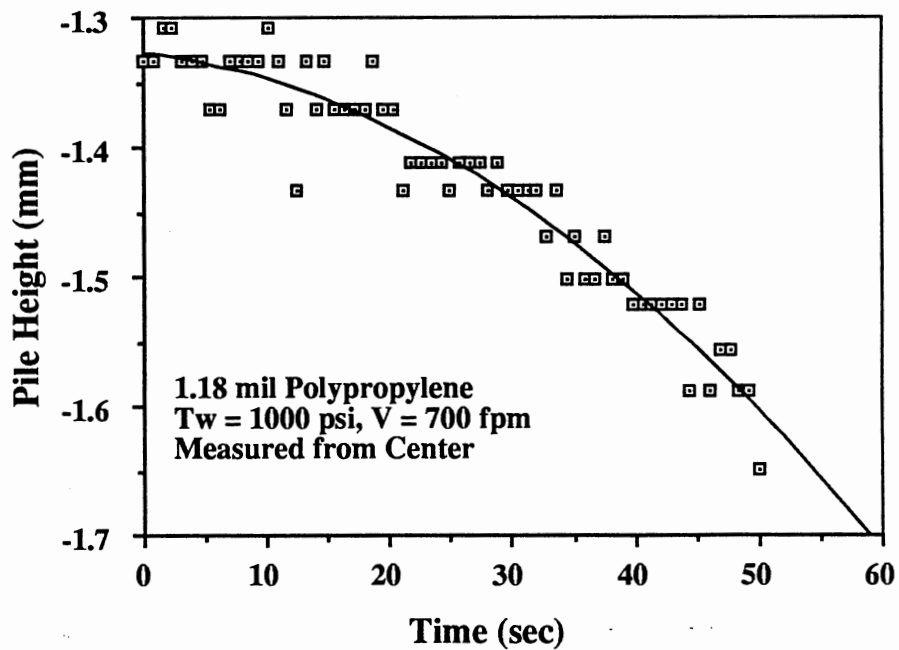


Figure 67. Depletion Regression for Wind at 700 fpm

$$PH = -0.38297 + 6.5720e-4(\text{Time}) - 2.9583e-5(\text{Time})^2 \quad R^2 = 0.233$$

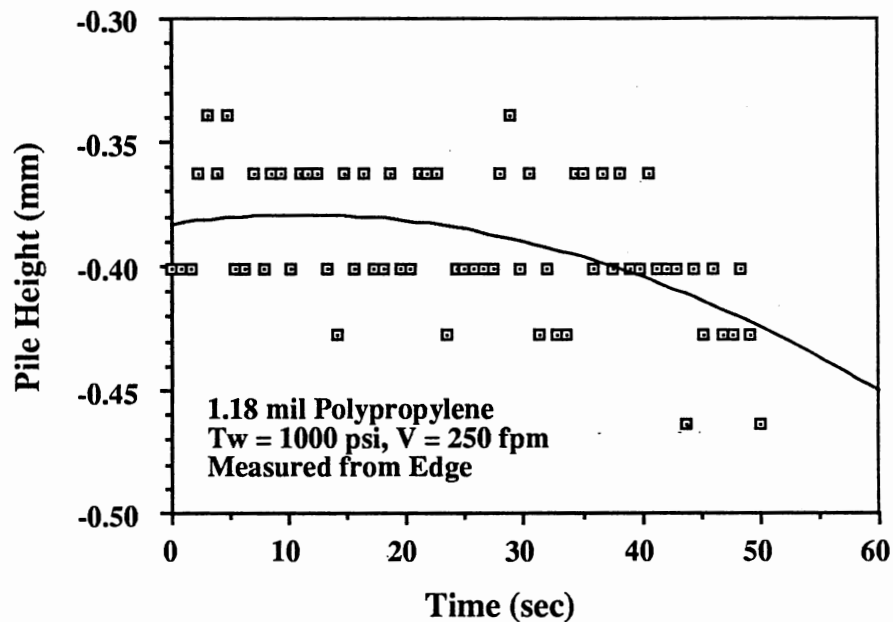


Figure 68. Depletion Regression for Wind at 250 fpm at Edge

$$PH = -1.3155 + 1.6791e-3(\text{Time}) - 1.0405e-4(\text{Time})^2 \quad R^2 = 0.845$$

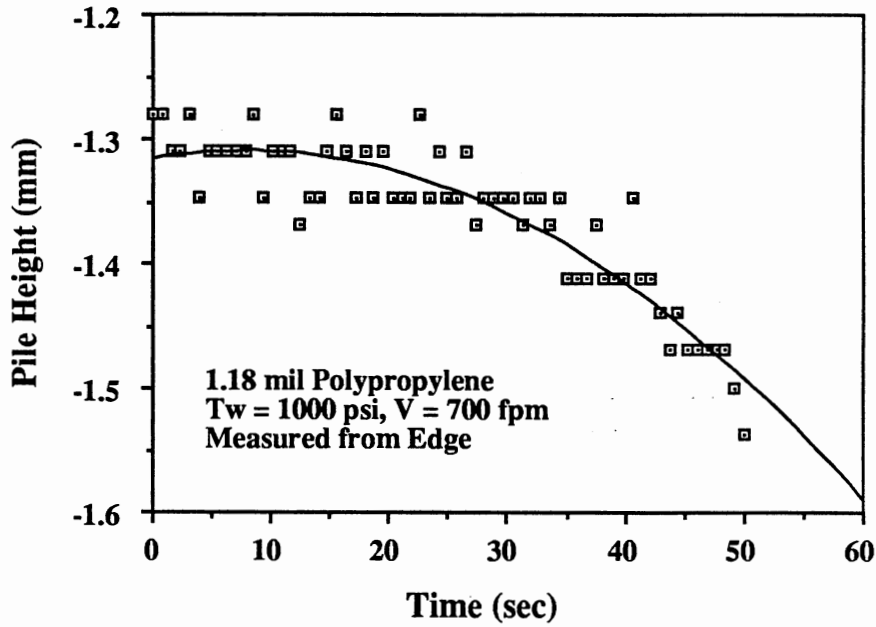


Figure 69. Depletion Regression for Wind at 700 fpm at Edge

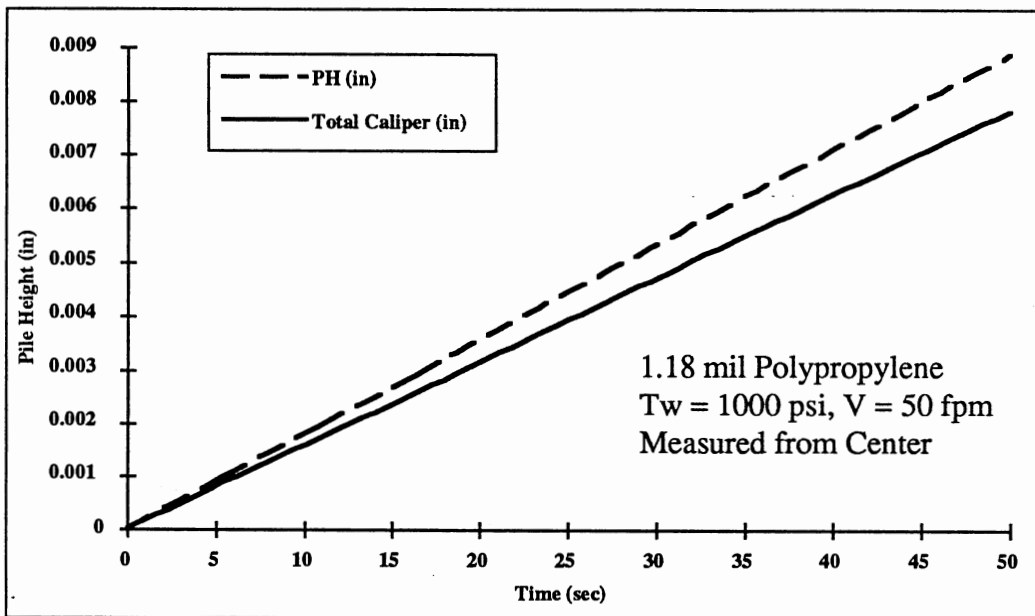


Figure 70. Pile Height Data for Wind at 50 fpm at Center

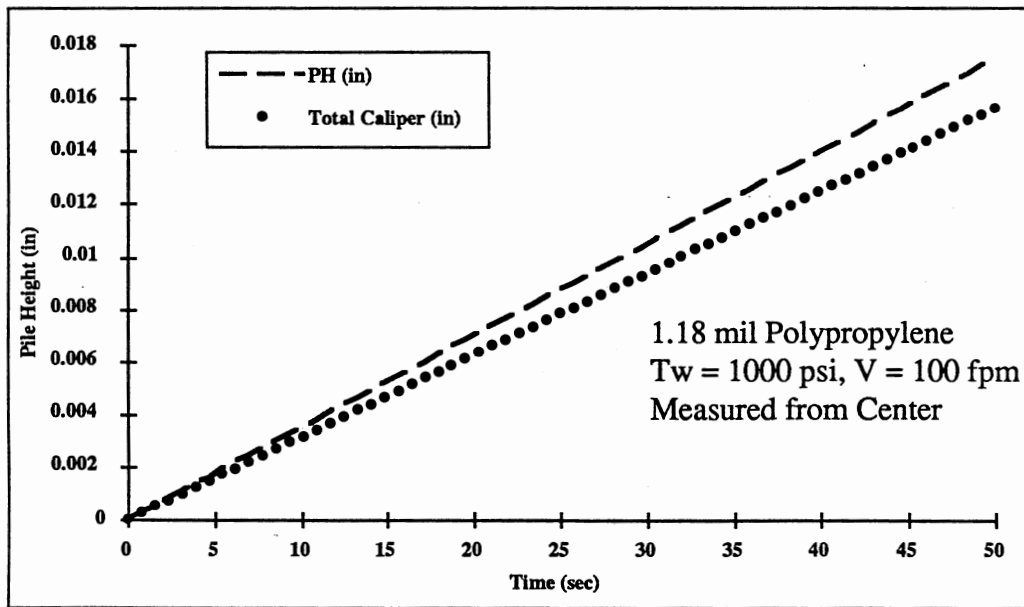


Figure 71. Pile Height Data for Wind at 100 fpm at Center

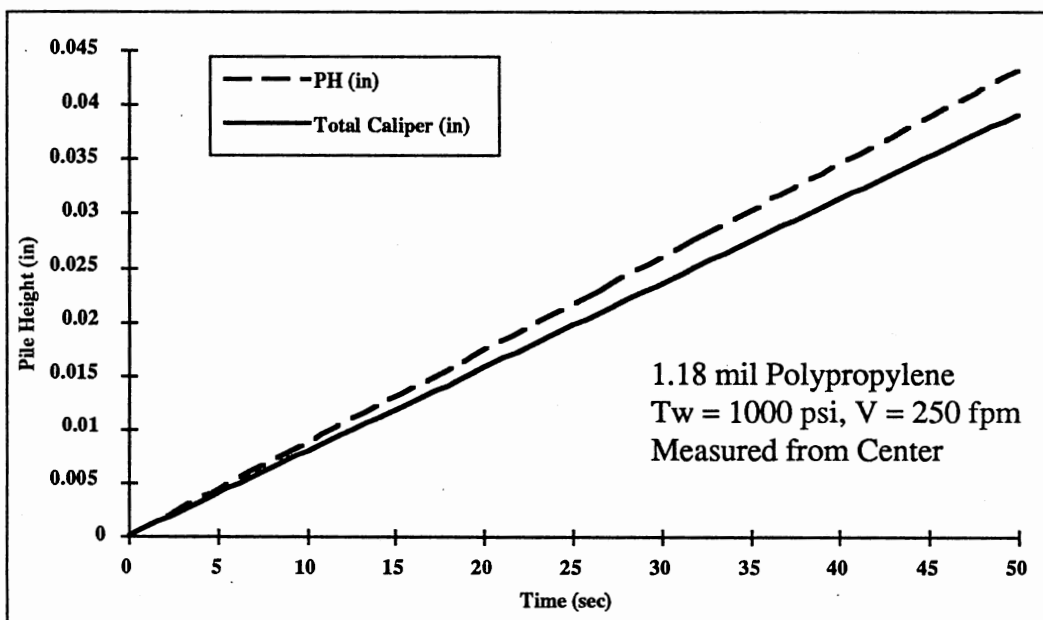


Figure 72. Pile Height Data for Wind at 250 fpm at Center

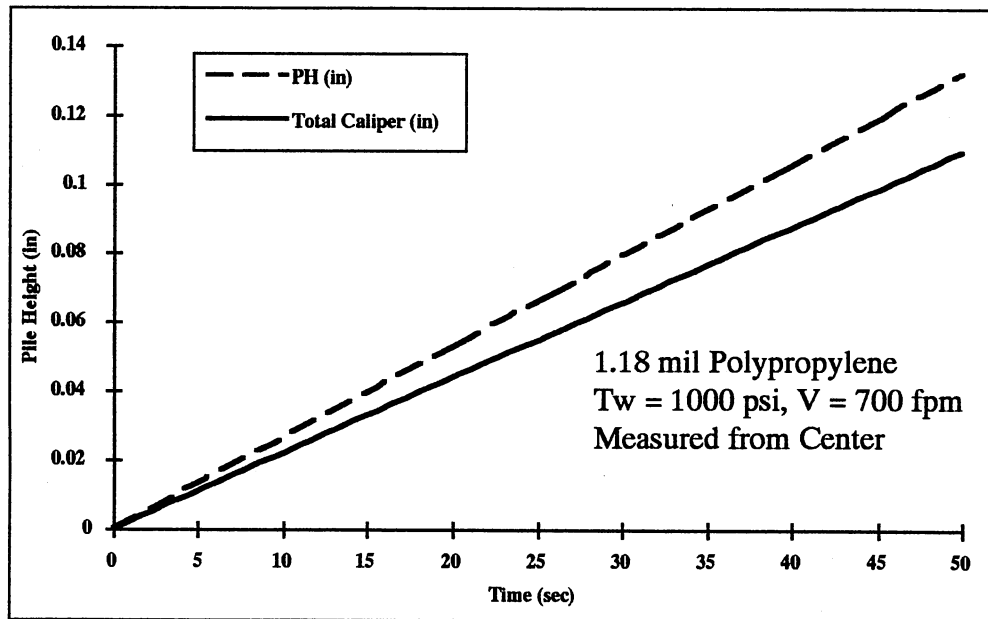


Figure 73. Pile Height Data for Wind at 700 fpm at Center

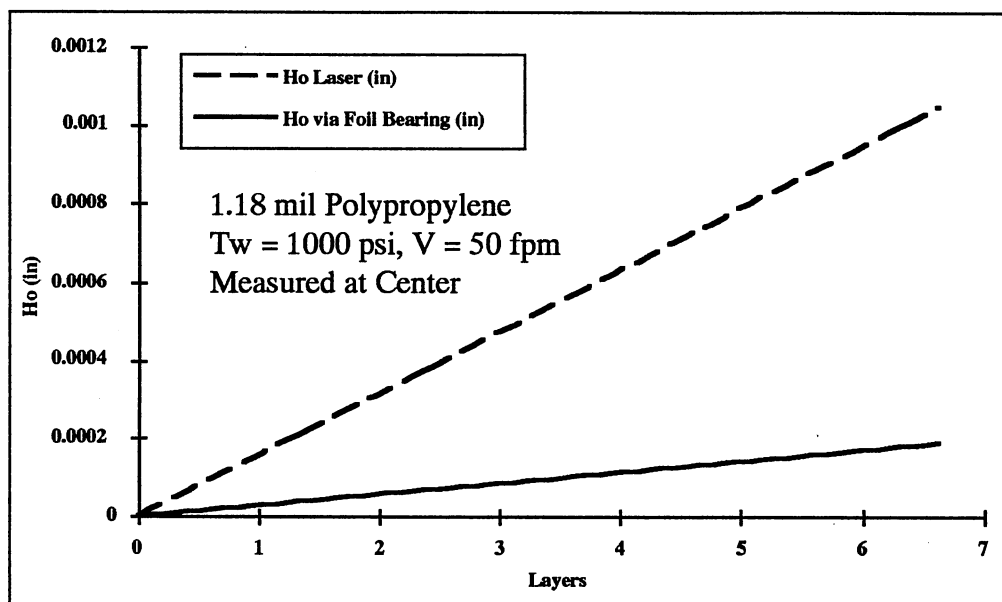


Figure 74. Comparison of Foil Bearing at 50 fpm at Center

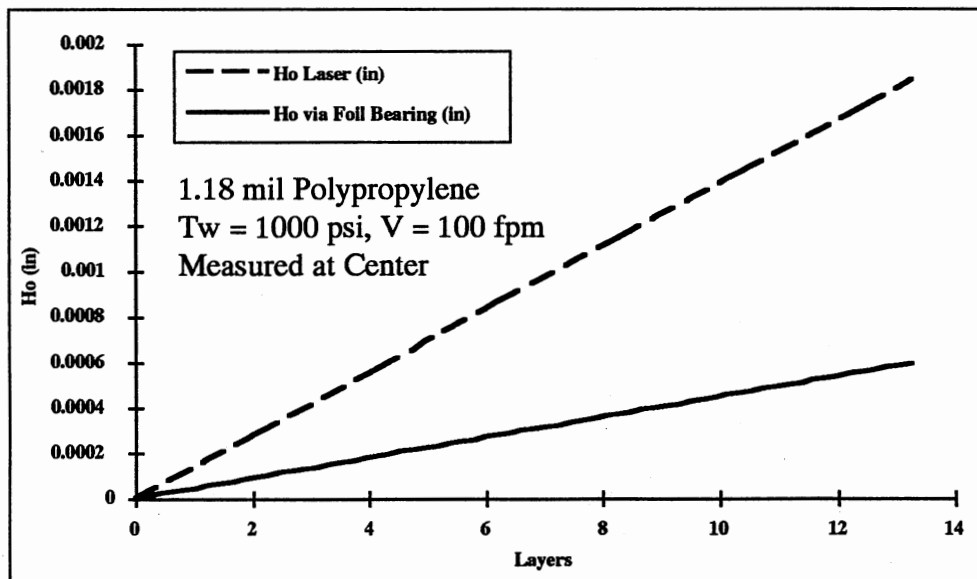


Figure 75. Comparison of Foil Bearing at 100 fpm at Center

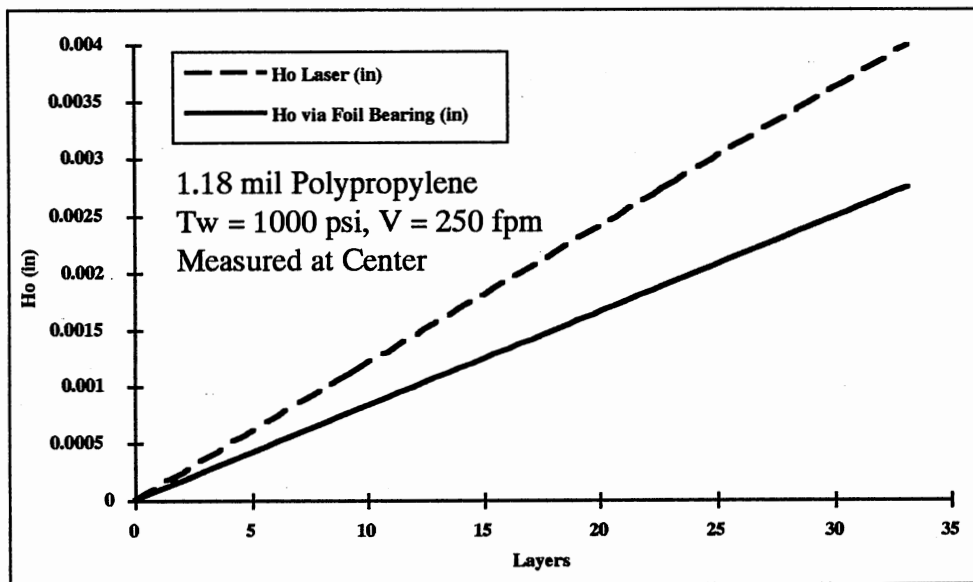


Figure 76. Comparison Foil Bearing at 250 fpm at Center

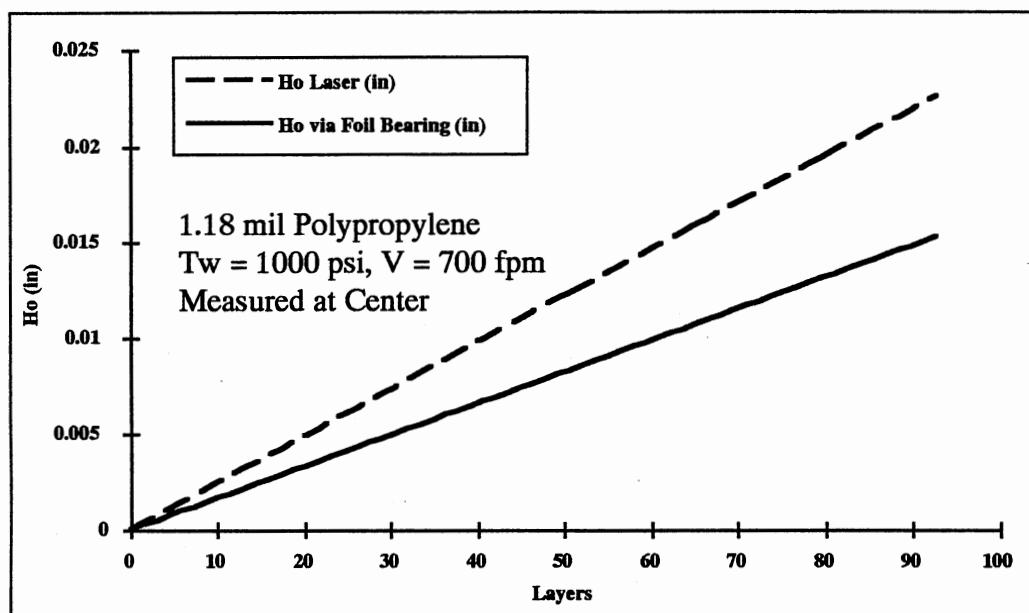


Figure 77. Comparison of Foil Bearing at 700 fpm at Center

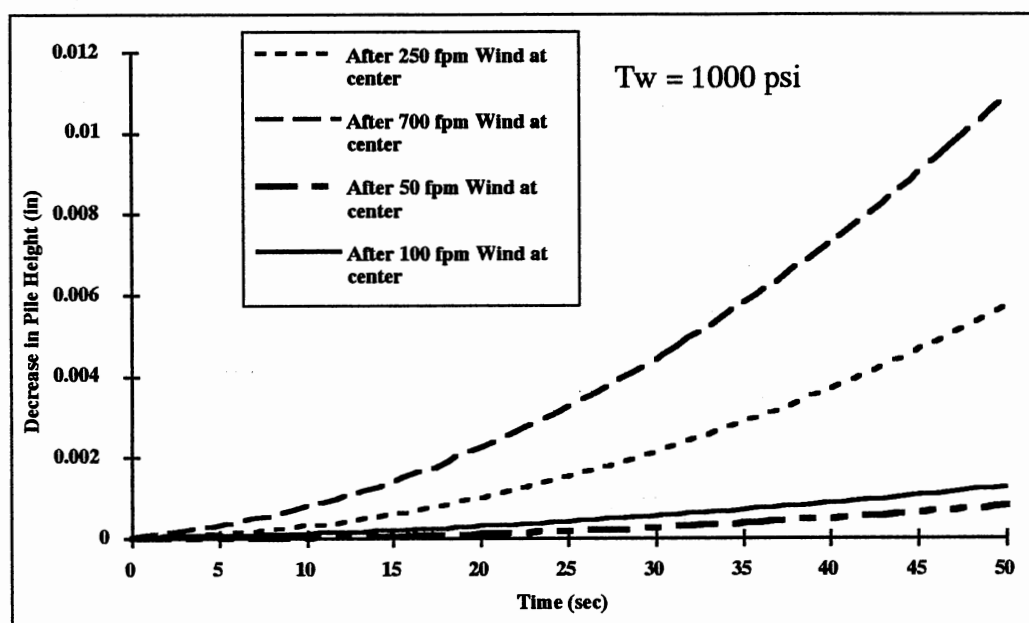


Figure 78. Depletion Data for Various Velocities Measured at Center

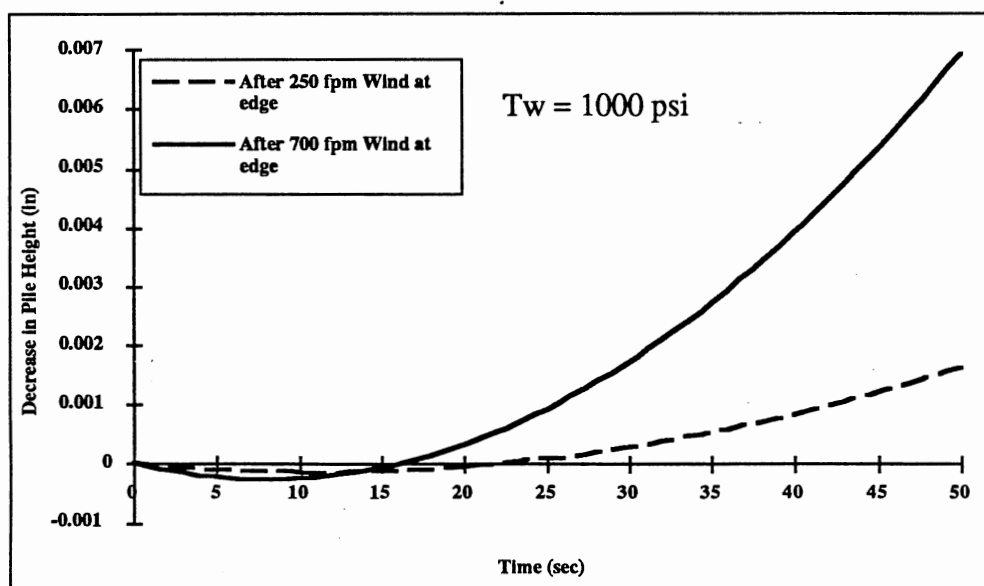


Figure 79. Depletion Data for Various Velocities Measured at Edge

VITA 

Michael William Holmberg

Candidate for the Degree of

Master of Science

Thesis: THEORETICAL AND EXPERIMENTAL STUDIES OF AIR ENTRAINMENT
IN WOUND ROLLS

Major Field: Mechanical Engineering

Biographical:

Personal Data: Born in Albuquerque, New Mexico, February 10, 1967, the son of Harold W. and Barbara J. Holmberg.

Education: Graduated from Edmond Memorial High School, Edmond, Oklahoma, in May 1985; received Bachelor of Science Degree in Mechanical Engineering from Oklahoma State University, Stillwater, Oklahoma, July 1990; completed requirements for the Master of Science Degree at Oklahoma State University in May 1992.

Work Experience: Research Assistant, School of Mechanical and Aerospace Engineering, Stillwater, Oklahoma, 1990-present.

Reservoir Engineer, Kerr McGee Corporation - U.S. on Shore Region, Oklahoma City, Oklahoma, May 1989 - August 1989.

Laboratory Assistant, School of Mechanical and Aerospace Engineering, Stillwater, Oklahoma, January 1989 - May 1989.

Student Engineer, San Bernardino Water Department, San Bernardino, California, May 1987 - August 1987.